9-3-2010

Metrology of optical telescope components

Ran Fu

Ran Fu

Candidate

Civil Engineering

Department

This thesis is approved, and it is acceptable in quality and form for publication:

Approved by the Thesis Committee:

Dr. Walter Gerstle , Chairperson

Dr. Arup Maji

Dr. John McGraw

Dr. Thomas Murphey

Metrology of Optical Telescope Components

by

Ran Fu

B.S., Tongji University, 2008

THESIS

Submitted in Partial Fulfillment of the
Requirements for the Degree of

Master of Science

Civil Engineering

The University of New Mexico
Albuquerque, New Mexico

July, 2010

Dedication

这篇论文献给我的家人和朋友们，感谢我的爸爸，妈妈的支持和鼓励，感谢雅轩和朋友们在我困难时候的陪伴。我会继续走下去。我深爱着你们。

To my father and mother, and my friends, for all the support and encouragement you have given to me. I hope that I can continue to make you proud. I love you.

Acknowledgments

I really appreciate Dr.Walter Gerstle, my advisor and defense chair, for giving me his trust by providing me the chance to pursue my M. S degree in the United States and work for him as a research assistant. I am deeply grateful to him, for his kindness, time and patience in helping me to fit into this new world during my study period. I have learnt a lot from his guidance in terms of academic achievement, professional style and personality. His guidance will remain with me as I continue my career as a Civil Engineer. Honestly, I had a great time working with Dr. Gerstle.

I also thank my committee members, Dr. Arup Maji, Dr. John McGraw and Dr. Thomas Murphey, for their valuable recommendations pertaining to this study and assistance in my professional development. Special thanks to Dr. John McGraw and Dr. Thomas Murphey for the funding to pursue this research.

I am grateful to all my close friends who always stood by my side and encouraged me throughout my time in graduate school and also in a different country. Thanks John, Karen, Valerie, Huimin, Ruoyu, Yongming, Tong, and Tu for everything.

I would like to extend my special gratitude to my girlfriend Darcy. Thank you for always being there and never letting me give up. It was my best time in my life when we were together.

And finally to my father and mother, Hong Fu and Ping Gao, your love is the greatest gift of all. I am the luckiest son in the world to have your eternal love.

Metrology of Optical Telescope Components

by

Ran Fu

ABSTRACT OF THESIS

Submitted in Partial Fulfillment of the
Requirements for the Degree of

Master of Science

Civil Engineering

The University of New Mexico
Albuquerque, New Mexico

July, 2010

Metrology of Optical Telescope Components

by

Ran Fu

B.A., Civil Engineering, Tongji University, 2008
M.S., Civil Engineering, University of New Mexico, 2010

Abstract

Precision astronomic structures such as telescopes often require structural materials that possess ultra low coefficient of thermal expansion (CTE) and coefficient of moisture expansion (CME) so that strict dimensional stability requirements can be met. Composite materials such as carbon fiber reinforced epoxy (CFRE) composites can meet those requirements because of their nearly-zero CTE and potentially low CME.

To employ these composite materials for telescope structural design, it is necessary to first develop practical and economical methods to determine their CTE and CME. Although many previous studies have discussed CTE and CME measurements of various materials, none of them suitably serve the purpose of measuring environmentally-

induced deformations of in situ telescope structural support members in terms of feasibility, repeatability and economy.

Two metrology techniques, suitable for measuring small deformations of large in situ telescope structural support members, have been developed for determining the CTE and CME of carbon fiber reinforced epoxy (CFRE) telescope components. Both are relative (rather than absolute) techniques, measuring the axial deformation of the telescope component with respect to a known reference standard. Two techniques are described: the single-mirror optical lever (SMOL) and the double-mirror optical lever (DMOL). In the first method, the temperature of the test component is varied while the reference standard is maintained at constant temperature, while in the second method the temperatures of the test component and the reference standard are varied together by changing the ambient temperature surrounding both. Quantitative CTE and CME results are reported for CFRE rods. Also, error analysis including random errors and systematic errors are discussed for each measurement. The magnitude of the error reflects the accuracy and reliability of the techniques.

The DMOL technique is shown to be a significant improvement upon the first and also more practical and economical than comparable techniques reported in the literature. We believe this DMOL method is superior to metrology methods for large telescope components published to date.

Contents

List of Figures

List of Tables

Chapter 1

Introduction

1.1 Objective

Many Earth- and space-based optical telescopes require optical elements to be positioned with tolerances on the order of microns or less, despite the fact that the structural supporting members may be constructed from a material with nonzero coefficient of thermal expansion (CTE) and nonzero coefficient of moisture expansion (CME). Modern materials and metrology are now beginning to allow this level of deformational precision, even without active control techniques.

However, structural materials, such as carbon fiber epoxy composites used to support optical elements, may possess low and even negative CTE and CME and are known to exhibit random and systematic spatial variations of CTE and CME. Thus it is desirable to develop tunable support struts that can be manually adjusted, especially in situ, to minimize motions of the optical components caused by temperature and humidity changes [1]. To achieve the goal of tuning telescope components in situ, it is first necessary to develop practical methods for measuring small deformations of the telescope components.

1.2 Background

Design of the CCD/Transit Instrument with Innovation Instrumentation (CTI-II) originally motivated this research. Although CTI-II funding is currently no longer available, the Air Force Research Laboratory continues to have an interest in this research.

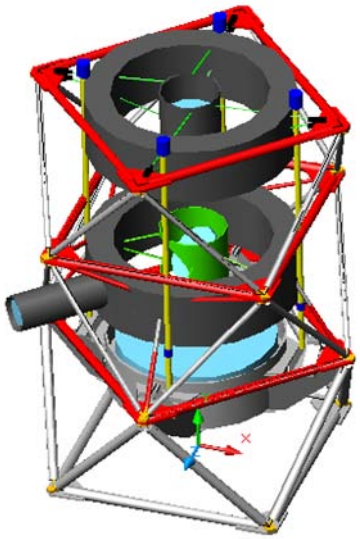

Figure 1-1. CTI - II optical telescope bent cassegrain configuration [1]

Because CTI-II shown in Figure 1-1 is stationary with respect to the earth, the design goal for CTI-II is to make the telescope as passive as possible so that it can remain stable despite environmental perturbations. Gerstle, Roybal, McGraw and Willams described these environmental loads in the paper “Structural Design of a Unique Passive Telescope” [1] which included:

(1) Atmospheric: wind, acoustic and barometric pressure change;

(2) Thermal: temperature change;

(3) Humidity: moisture change;

(4) Long-term material deformations: creep and shrinkage;

(5) Seismicity: earthquake, vibrations caused by machinery and human-caused deformation;

(6) Gravity: from other celestial bodies.

Roybal described the structural design of this passive telescope in his thesis "Structural Design of a Passive Transit Telescope" [2] in 2007. In his thesis, the design of CTI-II was introduced, and the finite element method (FEM) was used to analyze the structural performance under external pertubations such as wind loading, temperature change and vibration. Then a 1:1 scale test on the original CTI was presented in his work for the purpose of comparing and validating his structural analyses. In his thesis, the design of structural components to eliminate thermally induced deformations was explored. The investigation into zero CTE composites shows that a composite laminated structure can be designed to have either zero CTE in a one direction, or very small CTE in two directions. Finally, the effect of moisture expansion is shown to be the most influential environmental effect upon the composite material.

Roybal's suggested in his thesis is further investigation into carbon fiber reinforced epoxy (CFRE) composite material including its thermal and moisture properties. Therefore, laboratory tests that measure coefficient of thermal and moisture expansion are needed to complete the telescope structural design. This thesis focuses on the measurement of environmentally-induced small deformations of large telescope components made of carbon fiber reinforced epoxy (CFRE). These micron-level deformations are caused by temperature and moisture changes.

Several methods and techniques were evaluated for this purpose during the two-year investigation of this research, including optical-lever dilatometers, telescopes, microscopes and theodolites (or total stations), as alternative methods for metrology of small deformations of large in situ telescope components.

Particularly, two types of optical-lever dilatometers were developed and applied for the experimental verification. The first is called the single-mirror optical lever (SMOL) and the second is called the double-mirror optical lever (DMOL). The SMOL method is subsequently used for CTE measurement and the DMOL method is an important improvement upon the SMOL method. Ultimately, the DMOL is shown in this thesis to be a reliable and repeatable method for measuring both ultra low CTE and CME. The applications of these two methods are introduced respectively in Chapter 3, Chapter 4 and Chapter 5.

Beside these two main methods, other methods were also explored during our research. For instance, the theodolite, shown in Figure 1-2, is able to measure the length change $\Delta L = L_2 - L_1$ with respect to the angle change $\Delta\theta = \theta_2 - \theta_1$. In this investigation, it was confirmed that the best commercially available theodolites are able to measure angles within sub-arc second precision. The Kern E2 theodolite [3] supposedly has sub-arc second pointing and measuring resolution, and it can focus on objects at a distance of 1.5 m to infinity. However, after renting and testing this instrument, we found that it was unable to even resolve the micron-size divisions on a micrometer slide viewed at the closest possible focusing distance of 1.5 m. It thus became clear that using a commercially-available theodolite for metrology of optical telescope components is not currently practical.

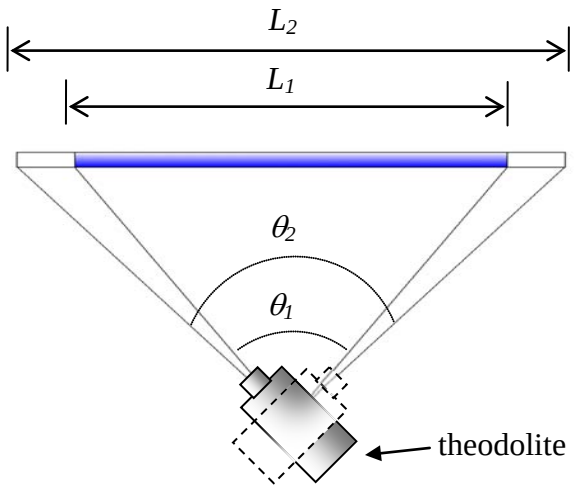

Figure 1-2. Schematic of theodolite (or total station) method

Microscopes were also tried for measuring small deformation, together with glass micrometer slides (Figure 1-3). Although a good microscope we can easily resolve the micron-size divisions on a micrometer slide (Figure 1-4), the focal distance is on the order of one centimeter or less. Thus a pair of microscopes positioned very accurately on a dimensionally-stable reference platform and also supporting the sample to be tested would be required to gain this focal distance and measure sample deformations. Again, we were unable to devise a practical method for metrology of large telescope components using microscopes.

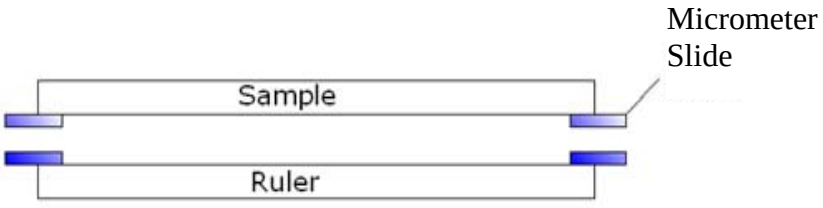

Figure 1-3. Schematic of micrometer slide method

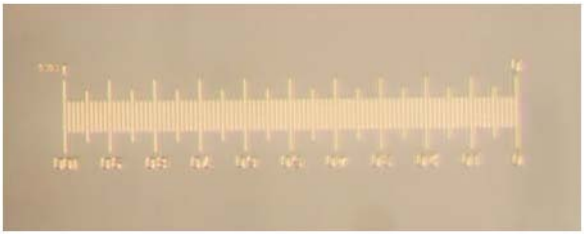

Figure 1-4. Observation of the micrometer slide through microscope

Finally, we considered purchasing a surgical microscope of the type (Figure 1-5) used by ophthalmologists. Such microscopes can resolve micron-level details at a distance of 10 cm but, again, a pair of such microscopes anchored to a dimensionally-stable reference platform would be required. This was found to be impractical for measurements.

Figure 1-5. Surgical microscope

Therefore, this thesis focuses upon the introduction and application of single-mirror optical lever (SMOL) and double-mirror optical lever (DMOL) techniques, as described in the following chapters.

1.3 Scope

This thesis is divided into six chapters.

Chapter 1, *Introduction*, discusses the background of the Passive Transit Telescope as well as the research purpose in measuring environmentally-induced deformations of telescopes components which are made of carbon fiber reinforced epoxy (CFRE) composite materials. In this chapter, several other unsuccessful methods and techniques are also introduced because they were carefully considered and evaluated during the research exploration.

Chapter 2, *Literature Review*, focuses on a review of various empirical metrology methods having been employed in the measurement of thermal and moisture expansion in the literature. Several reliable and high-precision methods are described including mechanical dilatometry, optical interferometry and strain gages. In the end, a summary table is provided to compose methods. Throughout the review and understanding of these existing practical metrology methods, it is found that it is necessary to find a more practical method of measurement of environmentally-induced small deformations of large telescopes components.

Chapter 3, *Experiment I: Measurement of C oefficient of Thermal Expansion Using Single-Mirror Optical Lever (SMOL)*, describes the first experiment on measuring CTE of a low-expansion material: IM7 carbon fiber reinforced epoxy (CFRE). The SMOL setup is developed for measuring the CTE of large telescope components. Error analysis is also included for providing both random and systematic errors to each measured CTE value. However, the SMOL method is found to be inaccurate due to the large systematic errors.

Chapter 4, *Experiment II: Measurement of Coefficient of Thermal Expansion Using Double-Mirror Optical Lever (DMOL)*, presents an improved method, based on the previous SMOL setup, called the double-mirror optical lever (DMOL). This method is independently developed for better measuring the CTE of CFRE, because it introduces a double-mirror arrangement for improving the magnification and reducing systematic errors. Also, a temperature-controlled chamber is used to obtain a spatially uniform temperature. To improve the accuracy of DMOL apparatus, both random and systematic errors are considered as well.

Chapter 5, *Experiment III: Measurement of Coefficient of Moisture Expansion Using Double-Mirror Optical Lever (DMOL)*, describes the application of the DMOL setup for measuring the Coefficient of Moisture Expansion (CME). Using the DMOL setup, tests of "Strain versus Exposure Time" and "Moisture Desorption versus Exposure Time" are separately conducted to explore the sample's strain and weight changes due to the desorption process in the environmental chamber. Finally, a linear relationship between strain and moisture desorption and thus the CME of the sample is found.

Chapter 6, *Conclusions*, presents the summary of these three experiments and two measuring methods including SMOL and DMOL. The conclusions and suggestions for future work are given.

References are also provided at the end of the thesis.

Chapter 2

Literature Review

2.1 Introduction

The dimensional changes produced in materials by t emperature and moisture variations are generally very small, so that sensitive measuring techniques must be used to observe them. In the history of metrology, a great variety of empirical methods have been employed in the measurement of thermal and moisture expansion, and the main purpose of this chapter is devoted to a review of these techniques, with particular reference to their accuracies and their scope of. Reference is also made to some of the standards in existence for thermal and moisture expansion measurement. This brief review of existing methods for thermal and moisture measurement shows that the three main methods include: mechanical dilatometry, optical interferometry, and strain gage techniques.

2.2 Review of Measurement Techniques

Mechanical dilatometry

Mechanical dilatometry techniques are the oldest and most widely used methods for measurement of thermal expansion. Mechanical dilatometer facilities are available for the measurement of fractional length change as a function of temperature, from which the derived mean linear expansion coefficient over a t emperature range or t he tangent expansivity at a given temperature can be computed [4].

With mechanical dilatometry, a specimen is placed in a temperature-controlled chamber and heated gradually. The displacement of one end of the specimen is mechanically transmitted to a sensor by means of a contacting component such as a push-rod. During the temperature change of the sample, the sensor and contacting component are kept away from the heat. Thus, the CTE of the sample can be calculated by measuring the displacement of the contacting component as a function of temperature.

A push-rod is frequently used as the contacting component to determine the change in length of a solid material. The specimen is placed in a closed tube after making certain that all contacting surfaces are free of foreign materials. Care must be taken to assure good seating of the specimen against the tube bottom and the push-rod, shown in Figure 2-1 [5].

The assembled dilatometer is placed into the environmental chamber, furnace, or other temperature-controlled environment and the temperature of the specimen is allowed to come to equilibrium. The rod protrudes from the controlled temperature environment to a contact displacement sensor such as a *linear variable differential transformer*

(LVDT), which is maintained at ambient temperature. The increase in distance *x* is the measured as a function of temperature.

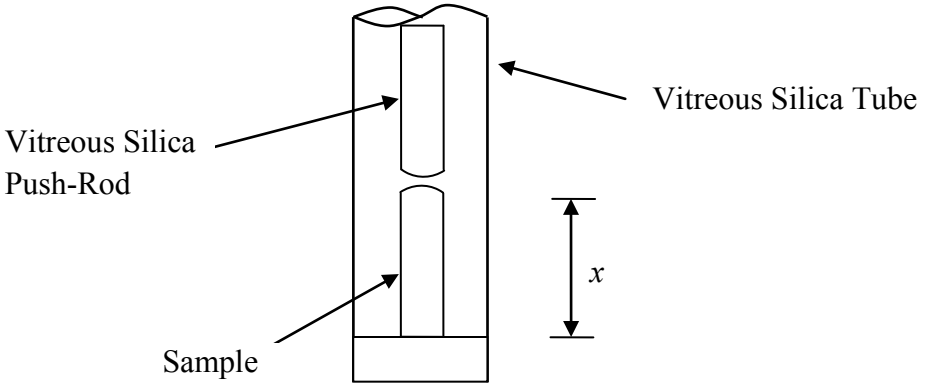

Figure 2-1. Schematic of mechanical dilatometer described in ASTM Test Method E 228 [5]

The rod protrudes from the controlled temperature environment to a displacement sensor such as a *linear variable differential transformer* (LVDT), which is maintained at ambient temperature. The increase in distance *x* is measured as a function of temperature.

Because the length of the push-rod may change during the temperature change, the push-rod's phase change or response to stress (elastic, plastic or creep deformation) must be taken into consideration. Consequently, the accuracy of this apparatus is critically dependent on the material selected for construction of the push-rod. The most suitable push-rods are vitreous silica, high-purity alumina and isotropic graphite. ASTM Test Method E 228 [5] describes the determination of linear thermal expansion of rigid solid materials using vitreous silica push rods or tube dilatometers.

The typical mechanical dilatometer tube can also be made of vitreous silica [6]. Vitreous silica, similar to fused silica and quartz, in the amorphous state has a very low

coefficient of thermal expansion (CTE), about 0.5×10^{-6} / °C. However, at about 1000 °C, this material will change from an amorphous state to a crystalline state, which has a much higher CTE. Therefore, the temperature limit of the vitreous silica rod dilatometer is up to 1000 °C [6]. For higher temperatures, polycrystalline alumina may be employed [7][8]. Alumina rod-systems can extend the temperature range up to 1600 ° C (2900 °F) and graphite rod-systems up to 2500 °C (4500 °F)[9].

Contact between the push rod and the specimen is another important factor to be considered. The contacting surfaces must be either flat or rounded to a large radius. Pointed ends should be avoided as these can lead to local deformation. If amorphous silica push rods are used, one must make sure to clean the surfaces carefully. For instance, using alcohol to avoid devitrivication [10], and direct contact with the hands should be avoided.

Dilatometers also differ in their placement directions: horizontal or vertical [4]. Many dilatometers are mounted horizontally, as this gives better temperature uniformity within the furnace. In these cases a small compressive force is applied to the push-rod to ensure good contact between the specimen and push-rod. This is especially important where measurements are to be made on cooling, as there is a danger of losing contact as the components contract. In contrast, components in a vertical dilatometer can remain in contact under their own weight, which may be at the expense of an inferior thermal gradient in the specimen due to furnace convection currents. A vertical push-rod dilatometer has been used to measure the expansion of specimens undergoing sintering [11] at temperature of up to 1500 °C with an accuracy of 1 μm. In some cases this was taken to a temperature where the sample was partly molten.

Optical Interferometry

The use of interferometry to measure length change directly from the test-piece is less common but potentially more accurate than mechanical dilatometry because it is less reliant on mechanical contact. Although the concept of optical interferometry is relatively straightforward, the technique is expensive due to elaborate equipment requirements, limited in temperature range, and restrictive in terms of test-piece type and geometry. By employing sophisticated instrumentation, it is possible to achieve great accuracy with these absolute techniques. The accuracy of this type of arrangement allows perhaps an order of magnitude improvement over mechanical dilatometry, but is limited by achievable temperature homogeneity. The precision can also be considerably better than that of mechanical dilatometry [12].

Optical interferometry works because when two waves with the same frequency combine, the resulting interference pattern is determined by the phase difference between the two waves. A typical arrangement is shown in Figure 2-2. The specimen S is placed on an optical flat mirror (A) and has an optical flat placed on top (B). The flats move apart or together as the specimen expands or shrinks. Rays reflect from the bottom surface α of the upper flat (which is transparent) and the top surface β of the lower flat. Constructive interference occurs if the transmitted beams are in phase, and this corresponds to a high-transmission peak. If the transmitted beams are out-of-phase, destructive interference occurs and this corresponds to a transmission minimum. Most interferometers use light or some other form of electromagnetic wave [13].

The specimen and optical flat system are positioned in a suitable heating system such as the furnace (or cryostat if low temperature properties are required). A vacuum

chamber is required in this system to give absolute measures of displacement. Therefore, no correction for the effect of the refractive index of the atmosphere on the wavelength of light is required. The increase in distance *x* is measured as a function of temperature

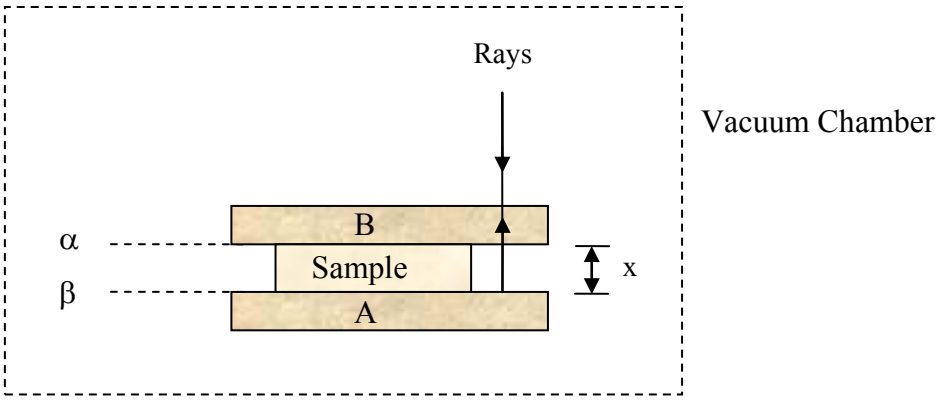

Figure 2-2. Schematic of optical interferometers with sample

Optical interference techniques for the measurement of thermal expansion mainly include Fabry–Perot, Fizeau, Moiré and Michelson interferometers, described next.

A Fabry–Perot interferometer (or etalon) [14] is typically made of a transparent plate with two reflecting surfaces, or two parallel highly reflecting mirrors. Its transmission spectrum as a function of wavelength exhibits peaks of large transmission corresponding to resonances of the interferometer. This interferometer makes use of multiple reflections of light between two closely spaced partially silvered surfaces. Part of the light is transmitted each time the light reaches the second surface, resulting in multiple offset beams which interfere with each other (Figure 2-3). Whether the multiply-reflected beams are in-phase or not depends on the wavelength (λ) of the light (in vacuum), the angle the light travels through the interferometer (θ), the thickness of the interferometer (*l*) and the refractive index of the material between the reflecting surfaces (n).

The large number of interfering rays produces an interferometer with extremely high resolution.

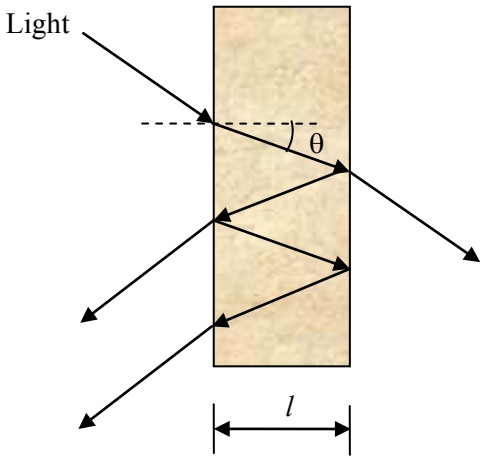

Figure 2-3. Fabry–Pérot interferometer [15].

A Fizeau interferometer is similar to a Fabry–Pérot interferometer in that they both consist of two reflecting surfaces [16]. In a Fizeau interferometer, however, the two surfaces are usually much less than totally reflecting, so that secondary reflections do not contribute greatly to the fringe contrast. An angled beam splitter captures the reference and measurement beams. Fizeau interferometers are commonly used for measuring the shape of an optical surface. Also, it is usually used for CTE of small samples [17, 18].

Moire interferometry is a whole-field quantitative optical method for determining the in-plane displacement field of an opaque body. This method of experimental mechanics has high sensitivity, excellent fringe contrast, high spatial resolution, and extensive range. Its pattern location is coincident with specimen and it is real-time [19]. It is especially effective for non-uniform in-plane deformation measurements and has been

used in the research and development of microelectronic packages to measure thermally induced displacement fields [20].

The Michelson interferometer (Figure 2-4) [21] produces interference fringes by splitting a beam of monochromatic light so that one beam strikes a fixed mirror and the other a movable mirror. When the reflected beams are brought back together, an interference pattern occurs. Precise distance measurements can be made with the Michelson interferometer by moving the mirror and counting the interference fringes which move by a reference point. The use of Michelson interferometry permits deformation measurements with sub-micrometer accuracy for arbitrary sized or shaped samples. Maintenance of specular surfaces at high temperatures requires exceptional vacuum conditions and protection from vaporizing or degassing furnace components.

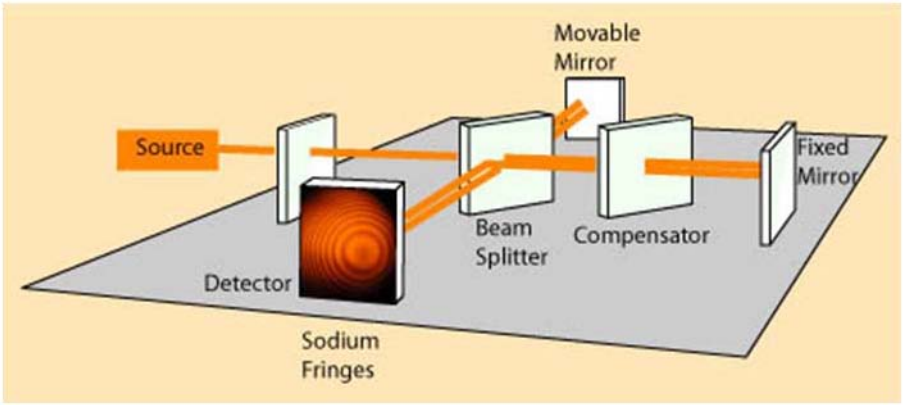

Figure 2-4. Michelson interferometer theory [21]

Strain Gages

A typical strain gage is a resistor in which the resistance changes with strain, shown in Figure 2-5 [22]. It is attached to the sample by a suitable adhesive, such as cyanoacrylate. When the sample is deformed, the strain gage is deformed as well, causing

its electrical resistance to change. Therefore the strain gage is sensitive to that small change in geometry. For a typical foil strain gage, the gage is far more sensitive to strain in the vertical direction than in the horizontal direction. The markings outside the active area help to align the gage during installation.

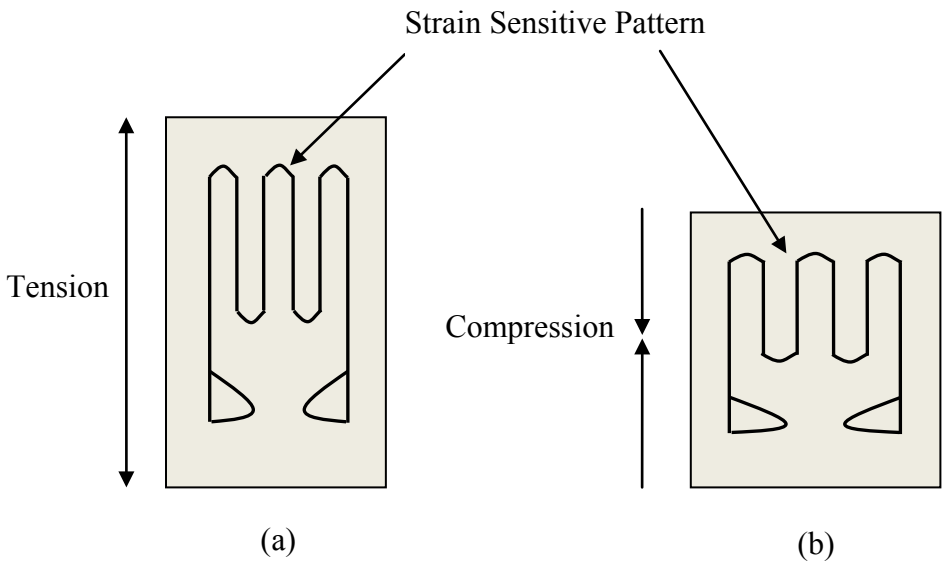

(a) When it is tension, area norrows, and resistence increases

(b) When it is compression, arrea thickens, and resistence decreases

Figure 2-5. Foil strain gage

Variations in temperature will cause an effect on the strain gage, because the sample changes in size by thermal expansion which will be detected as a strain by the gage. Most strain gauges are made from a constantan alloy which has been designed so that the temperature effects on the resistance of the strain gage itself cancel out and the resistance change of the gage is due only to the thermal expansion of the sample under

test [23]. High measurement accuracy (±0.05%) and resolution (0.5 micro-strain) can be achieved using the Vishay Micro-Measurements System [24].

2.3 Summary of Length Measurement Techniques

Table 2-1 shows a range of measurement techniques that cover the sample's dimensional requirements, resolution, accuracy and their relative costs.

Table 2-1. Summary of length measurement techniques [25]

Techniques	Resolution	Accuracy	For Large Sample Dimension	Device & Operation Cost
Mechanical Dilatometry	2×10^{-6} m	10^{-8} m	No	Low~ Medium
Optical Interferometry	10^{-7}~10^{-9} m	10^{-7}~10^{-8} m	No	High
Strain Gages	10^{-7}~10^{-9} (ε)	10^{-7}~10^{-8} (ε)	Yes	Low

Although mechanical dilatometry and optical interferometry both have relatively high resolution and accuracy, they cannot be used for measurement of large samples (such as telescope components). Also, the apparatus of optical interferometry becomes very complex when it is used for CME measurement [25]. As for strain gages, they provide only local deformation measurements. However we wish to measure the overall deformation of component. Also, strain gages are not practical for measuring CME because during the CME test expansion of hygroscopic adhesives and interference with moisture transport might cause problems. Therefore, exploring more practical and

specific methods is necessary for our purpose: measurement of environmentally-induced small deformations of large telescopes components. The next chapter will introduce a technique called the single-mirror optical lever (SMOL) technique.

Chapter 3

Experiment I: Measurement of Coefficient of Thermal Expansion Using Single-Mirror Optical Lever (SMOL)

3.1 Introduction

The coefficient of linear thermal expansion of a material or component can be defined as the fractional increase in length (strain) per unit rise in temperature. The SI units of this quantity are strain per ^{o}C or per K. The most general definition of the coefficient of linear thermal expansion is the average expansion over a temperature range, given by ASTM [5]:

$$\alpha_r = \frac{(L_2 - L_1)/L_1}{T_2 - T_1} = \frac{1}{L_1}\frac{\Delta L}{\Delta T} \quad , \qquad \text{Eq. 3-1}$$

where, L_1 is the initial length of the sample; T_1 is the initial temperature of the sample; L_2 is the ending length of the sample; and T_2 is the ending temperature of the sample.

α_r can be computed using the slope of the chord between two points on the temperature versus length curve (Figure 3-1). The coefficient of linear thermal expansion α represents the expansion over a particular temperature range from T_1 to T_2.

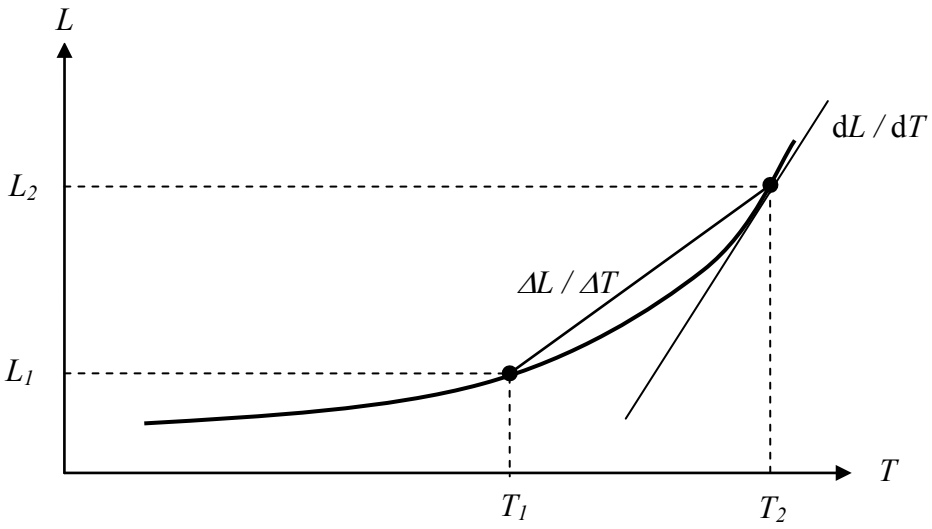

Figure 3-1. Change of length, L, of sample as a function of temperature, T [4]

Another definition for the coefficient of linear thermal expansion is related to derivative d*L*/d*T* at a single temperature. This is the slope of the tangent to the temperature verse length curve (Figure 3-1). This definition can be described as follows:

$$\alpha_s = \frac{dL/L_1}{dT} = \frac{1}{L_1}\frac{dL}{dT} \quad , \qquad \text{Eq. 3-2}$$

Eq. 3-2 actually is the limit of Eq. 3-1 when T_1 - T_2 approaches zero. The CTE defined over a temperature range α_r (Eq. 3-1) is different from that defined at a single temperature α_s. But for most materials at the room temperature range (10°C ~ 30°C), the CTE values from these two definition are almost the same [4].

For the volumetric expansion, the expansion is quantified in terms of the fractional increase in volume per unit temperature rise. The corresponding relationships are as follows [26]:

$$\beta = \frac{(V_2 - V_1)/V_1}{T_2 - T_1} \cong \frac{1}{V_1}\frac{\Delta V}{\Delta T} \quad , \qquad \text{Eq. 3-3}$$

where, V_1 is the initial volume of the sample; T_1 is the initial temperature of the sample; V_2 is the ending volume of the sample; and T_2 is the ending temperature of the sample.

β is defined as the coefficient of volumetric thermal expansion. The definition is usually applied to the thermal expansion of liquids and thus constant pressure is commonly required in this equation. For an isotropic material, β is equal to three times the coefficient of linear thermal expansion.

$$\beta = 3\alpha_s \quad , \qquad \text{Eq. 3-3}$$

In this thesis, the coefficient of thermal expansion is defined as α_r using a temperature range (Eq. 3-1).

In this chapter, we describe a device called the single-mirror optical lever (SMOL) for measuring the CTE in large telescope components. In this single mirror optical lever (SMOL) method, a mirror, supported by both the sample and the standard, tilts, causing a laser beam to be deflected, magnifying the deformation of the sample, as shown in Figure 3-2. This method, although independently developed, is similar to the laser-optical comparator (LOC) method described by Krumweide, Chamberlin and Derby [27]. The temperature of the sample is controlled by circulating ice water through an externally insulated sleeve encapsulating only the test component, and not the reference.

In addition, uncertainty in the measurement due to the random errors is computed and the commercial finite element analysis software ANSYS [28] is used to evaluate the systematic errors. In the end, a more reliable CTE value than the initial measured value based on the SMOL is achieved using a method described in the next chapter.

3.2 Theory and Equations for SMOL

The single-mirror optical lever (SMOL) is shown in Figure 3-2.

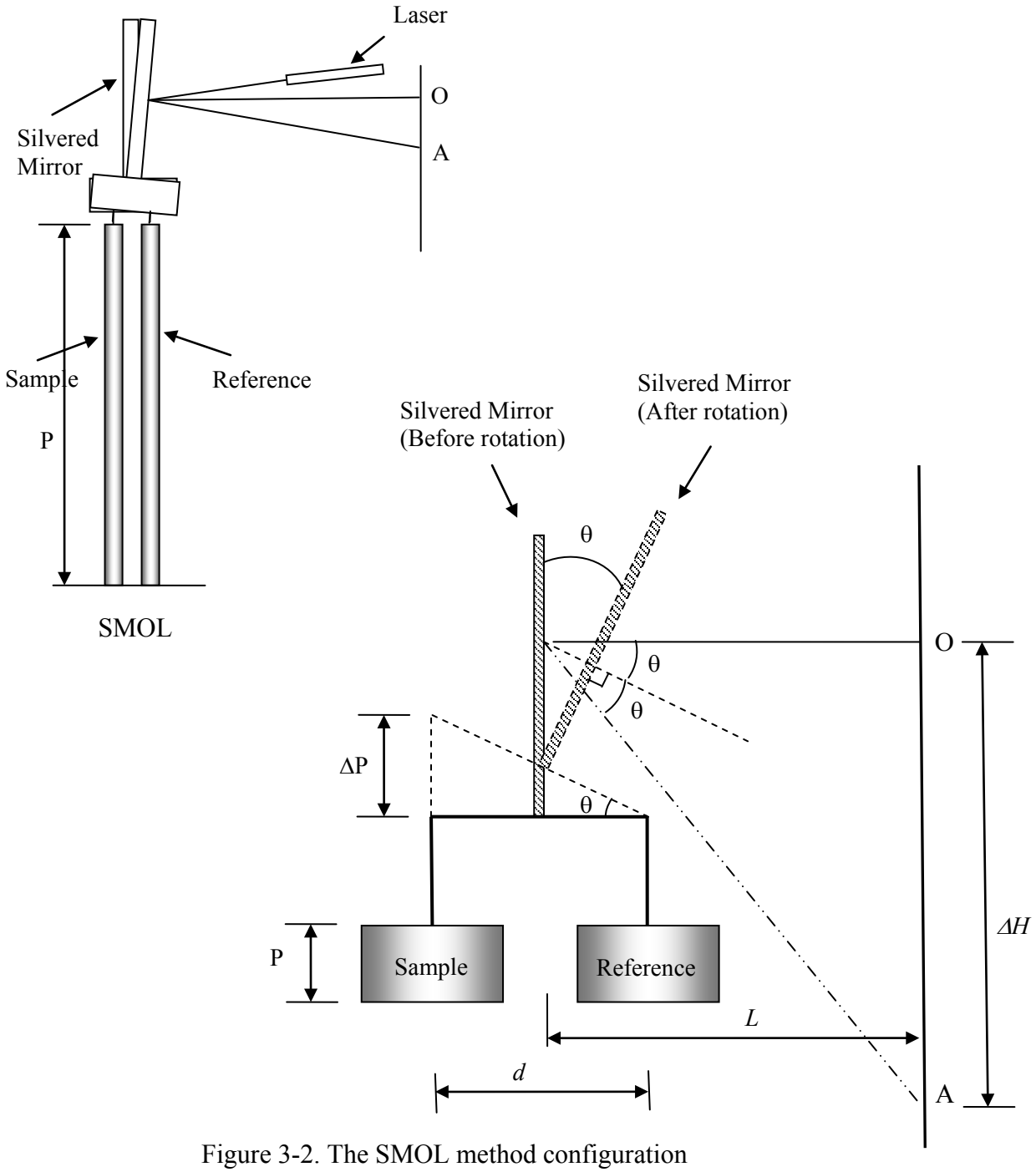

Figure 3-2. The SMOL method configuration

In Figure 3-2, when the sample deforms by ΔP, the mirror rotates by θ and consequently point O will be deflected to point A.

Using the small angle approximation [29]:

$$\tan\theta = \theta = \frac{\Delta P}{d} \text{ and } \tan 2\theta = 2\theta = \frac{\Delta H}{L} ,$$

Therefore, $$\frac{\Delta P}{d} = \frac{\Delta H}{2L} ,$$ Eq. 3-4

Eq. 3-1 can be represented as follows:

$$\alpha = \frac{\Delta P}{P \times (T_2 - T_1)} ,$$ Eq. 3-5

Eq. 3-4 and Eq. 3-5 yield:

$$\alpha = \frac{d}{(2L) \times P \times (T_2 - T_1)} \times \Delta H ,$$ Eq.3-6

where,

α is the coefficient of thermal expansion (CTE);

P is sample's original length (In this test, it equals 153.7 cm measured by ruler);

Δ*P* is the change of sample's length, shown in Figure 3-2;

T_1 is the temperature at beginning;

T_2 is the temperature at ending;

d is the horizontal distance between two mirror feet (In this test, it equals 1.0 cm, measured by ruler), shown in Figure 3-2 and Figure 3-3;

Δ*H* is the displacement of the laser point on the screen, namely distance between point O and point A, shown in Figure 3-2;

L is the horizontal distance between the flat mirror and screen (In this test, it equals 779.8 cm, measured by band tape), shown in Figure 3-2.

More details of the SMOL setup are provided in Figure 3-3. With reference to Figure 3-3, a temperature-adjustable sleeve (3) containing a sample (2) rests on the concrete floor (1). One footing of the flat mirror (4) is supported by the sample's top end; another footing rests on a ceramic support (5) which is supposed to serve as a reference because of the stable supporting platform. Water is circulated through the sleeve to change the temperature in the sleeve from room temperature (approximately 20 ^{o}C) to nearly 0 ^{o}C. Water doesn't contact the sample because there is an inner sleeve within which the sample resides and absorbs the heat from the air. In this SMOL system, the deformation of the sample due to the temperature change is measured via the optical lever, in which the flat mirror causes the beam from laser pointer (6) to be deflected. Therefore, a very slight motion (10^{-6} m to 10^{-7} m) of the sample with the change in temperature can be largely amplified to a visible laser spot motion (approximately 1 mm or larger) on the screen (8) due to the magnification (M).

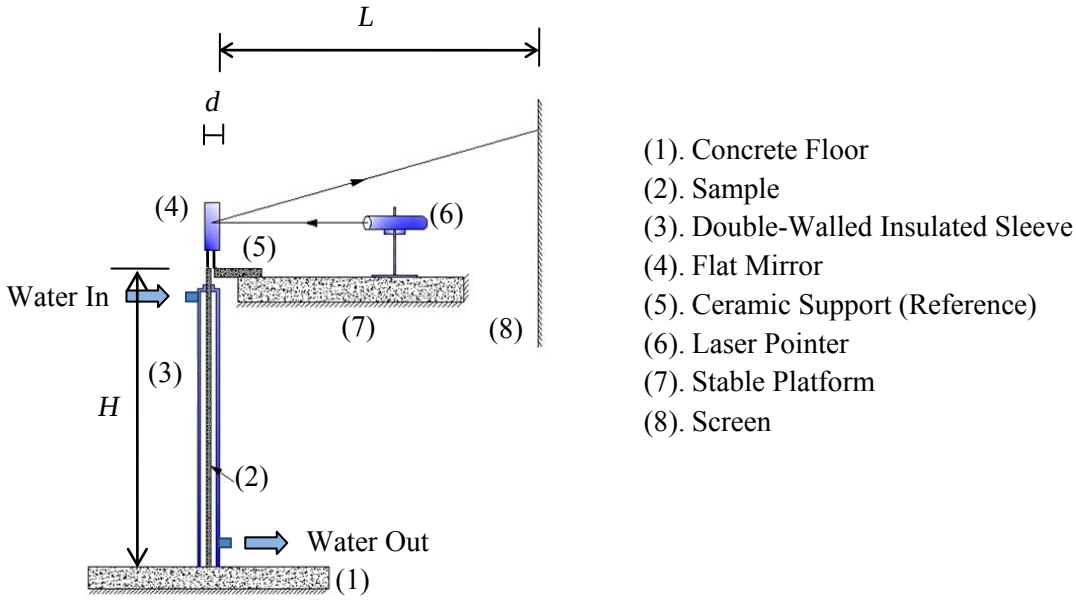

Figure 3-3. Schematic of the SMOL setup

The magnification (M) of the sample motion in the single-mirror optical lever (SMOL) is based on the distance of the laser path and the lever length of the mirror. For this SMOL system, $M = 2L/d = (2 \times 779.8\ cm)/(1.0\ cm) = 1560$.

Figure 3-4 shows several views of the SMOL setup and Figure 3-5 shows the details of the mirror assembly.

(a)

(b)

(c)

(a): Side view of mirror and supports

(b): Front view of mirror and supports

(c): Wooden shelf, laser pointer and water pipes

Figure 3-4. Photographs of the SMOL setup

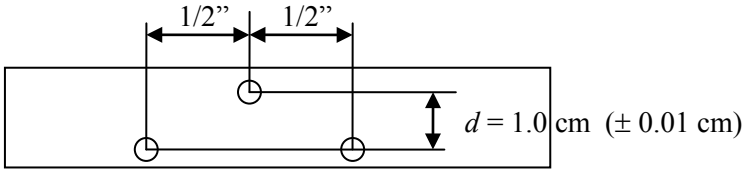

Top View of Three Footings

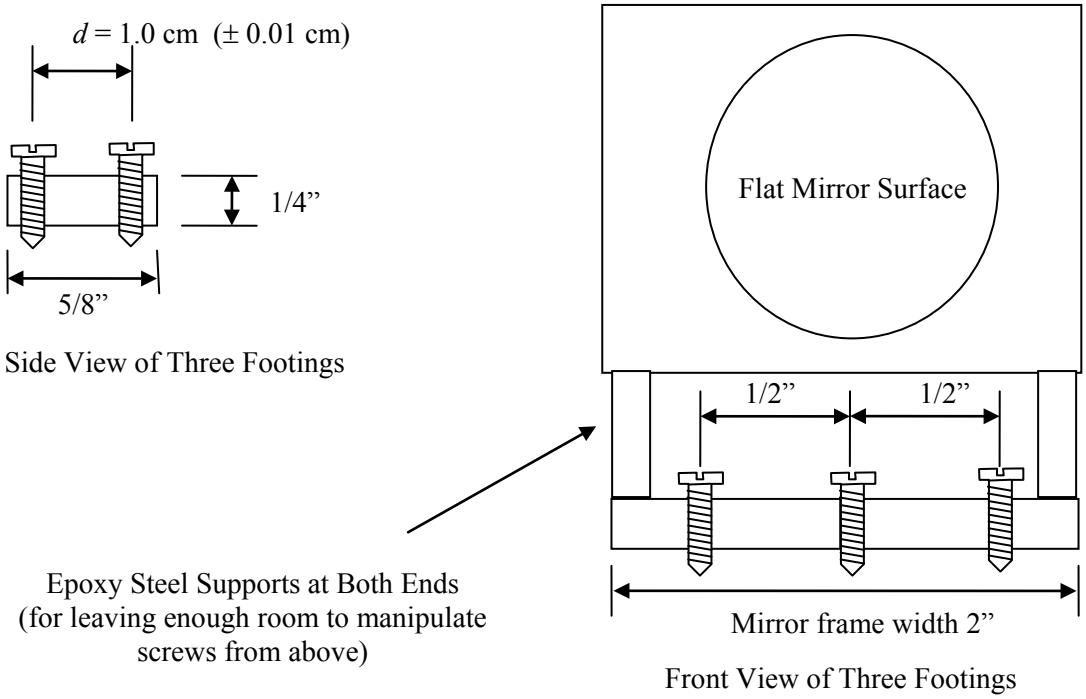

Side View of Three Footings

Front View of Three Footings

Figure 3-5. The flat mirror and its support

3.3 Operating Procedure for the SMOL Method

The detailed operating procedure for measuring CTE using the SMOL method is described as follows:

(1) Place sample in the double-walled insulated sleeve, avoiding the sample touching the inner surface of the sleeve;

(2) Start circulating the water through the sleeve in order to change the temperature of the sample. By adding ice water, the water circulation is able to keep the temperature at approximately 0 ^{o}C. This temperature decreasing process is defined as Phase 1; conversely, by adding the hot water, it is feasible to raise the temperature up to approximately 20 ^{o}C. This temperature increasing process is defined as Phase 2;

(3) Turn on the laser pointer when the test begins. Then adjust the flat mirror to reflect the laser spot upon the screen;

(4) During the test, mark the position of the laser spot at regular intervals as the temperature changes;

(5) Run the test until the temperature decreases from 20 ^{o}C to 0 ^{o}C (Phase 1) and then comes back to approximately 20 ^{o}C (Phase 2);

(6) The sample's CTE value can be computed using Eq. 3-6 according to the movement of the spot on the screen and the temperature change.

3.4 CTE Experimental Results from SMOL

In order to validate consistency and reliability, the tests are cycled from high temperature (approximately 20 ^{o}C) to low temperature (approximately 0 ^{o}C), which is Phase 1; and then conversely from low temperature to high temperature, which is Phase 2. Aluminum, stainless steel and IM7 carbon fiber reinforced epoxy (CFRE) are tested separately in this way. This is 3/8" CFRE rod. IM7 (InterMediate 7 modulus carbon fiber) indicates it has a Young's Modulus of 40-44 Million PSI. The rod was made from rolled-up pre-pregnated resin cloth, which is 32% resin, 68% carbon fiber. The cloth, after curing has a Young's Modulus of 24.5 Million PSI. The resin used is Hexel 8551-7A resin epoxy system.

The strain versus time and CTE results are shown in Figure 3-6, Figure 3-7 and Table 3-1.

Table 3-1. Aluminum, stainless steel and IM7 CFRE CTE results based on SMOL experiments (without considering random and systematic errors)

Sample	CTE (under 100^{o}C) from literature [30, 31] Per C×10^{-6}	CTE of Phase 1 Per C×10^{-6}	CTE of Phase 2 Per C×10^{-6}	CTE, average of Phases 1&2 Per C×10^{-6}
Aluminum	23 ~ 24	21.8	21.2	21.5
Stainless Steel	16.9 ~17.3	15.9	15.3	15.6
IM7 CFRE trial 1	- 0.64 (From Hexcel technical data sheets)	- 0.25	- 0.25	- 0.25
IM7 CFRE trial 2		- 0.23	- 0.25	- 0.24
IM7 CFRE trial 3		- 0.23	- 0.25	- 0.24

The results tabulated in Table 3-1 indicate that the measured CTE values of aluminum and stainless steel based on SMOL method are slightly lower than the range from the available literature. However, the differences are less than 10%. Also, the measuring errors including random and systematic errors are not considered in Table 3-1. The next section will discuss these errors.

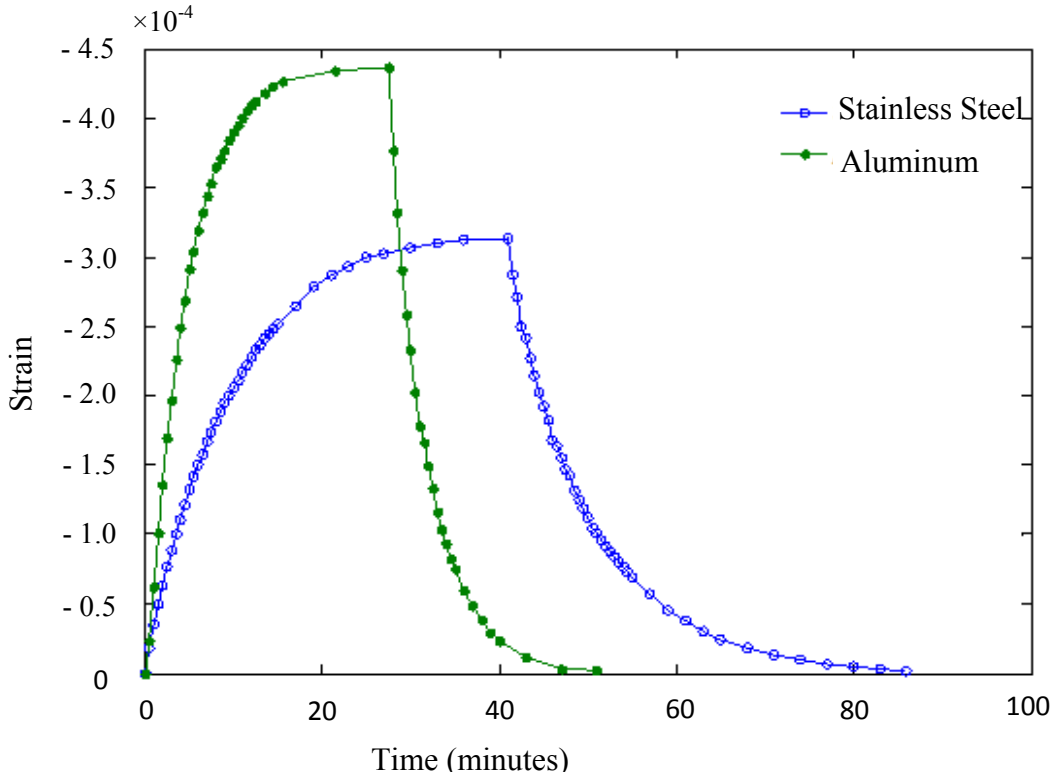

Figure 3-6. Strain versus time for aluminum and stainless steel tests

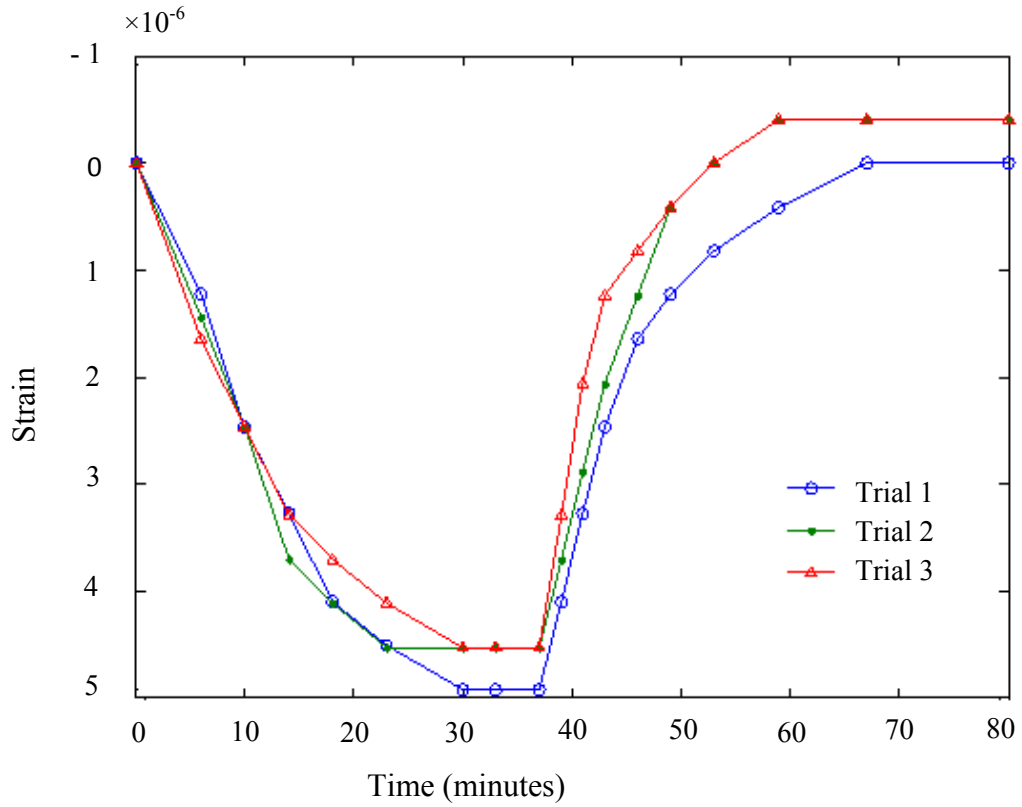

Figure 3-7. Strain versus time for three IM7 CFRE tests

3.5 Error Analysis of SMOL Tests

All quantitative measurements and any calculations using these measurements exhibit some degree of inaccuracy and uncertainty. These inaccuracies and uncertainties are both referred to as experimental error. In this thesis, the term "error" refers to a limitation caused by the observational method. It does not mean some careless mistake in measurement or computation; such "human" errors can be detected and eliminated by reviewing procedures and repeating the entire experiment [32].

There are two basic types of experimental error: *random* and *systematic* [33, 34].

(1) *Random errors* are caused by unknown and unpredictable changes in the experiment and cause the measured values to vary in a series of repetitions with the same experiments and observation.

Random errors are inherent and unpredictable. They are close to the true value, and their mean tends to approach a certain value when the measurement is repeated several times with the same instruments. As an example, random errors can be caused by unpredictable fluctuations in the reading of a measurement apparatus (e.g. mercury thermometer). The higher the precision of a measurement instrument, the smaller the variability of the fluctuations exists in its readings. In general, random error can be reduced by improving observational methods, but the fundamental sources of random error can never be completely eliminated.

(2) *Systematic errors* come from the measuring instruments in experimental observations and usually are constant in a series of repetitions with the same experiments and observation.

Systematic errors cannot be revealed by repeated measurements. Systematic errors always occur when we use the instrument in the same way. From a practical standpoint, systematic errors are usually more difficult to deal with than random errors, because their magnitude cannot be reduced by simple repetition of the measurement procedure multiple times.

3.5.1 Random Errors in the SMOL Tests

First, as for *random errors*, it is possible to quantify its magnitude using statistics. In this part, the notation $x \pm u\{x\}$ is used to represent an experimental result. x represents

the measured value from a single direct measurement; $u\{x\}$ is the estimated uncertainty for x by the experimenter of the readability of the instrument or a value taken from instrument specifications supplied by the manufacturer. To better demonstrate the uncertainty calculation procedure, measured data from aluminum CTE test (Phase 1) are taken as an example shown in Table 3-2.

Table 3-2. Measured values in aluminum CTE test (Phase 1) with their estimated uncertainties

Notation	Definition	Measured Value	Estimated Uncertainties
α	Coefficient of Thermal Expansion	／	／
d	Distance between two mirror footings	1.0 cm	± 0.1 cm
ΔH	Displacement of the laser spot on the screen (see Figure 3-2)	- 102.9 cm	± 0.3 cm
L	Distance between the flat mirror and screen (see Figure 3-2)	779.8 cm	± 1.0 cm
P	Sample's original length	153.7 cm	± 0.3 cm
T_1	Temperature at beginning	19.7 ^{o}C	± 0.1 ^{o}C
T_2	Temperature at ending	0.0 ^{o}C	± 0.1 ^{o}C

CTE calculation equation from section 3.2 is repeated below:

$$\alpha = \frac{d}{(2L)\times P\times (T_2 - T_1)} \times \Delta H \ , \qquad \text{Eq. 3-6}$$

The process of coming up with an expression to calculate α's uncertainty $u\{\alpha\}$ is called *uncertainty propagation*.

In the following we introduce the technique of general uncertainty analysis [35]. Consider a general case in which an experimental result, r, is a function of J measured variables X_i:

$$r = r(X_1, X_2, \ldots, X_j) \quad , \qquad \text{Eq.3-7}$$

Equation 3-7 is the data reduction equation used for determining r from the measured values of the X_i. Then the uncertainty in the result is given by:

$$u_r^2 = \left(\frac{\partial r}{\partial X_1}\right)^2 u_{X_1}^2 + \left(\frac{\partial r}{\partial X_2}\right)^2 u_{X_2}^2 + \cdots + \left(\frac{\partial r}{\partial X_j}\right)^2 u_{X_j}^2 \quad , \qquad \text{Eq. 3-8}$$

where u_{Xi} are the uncertainties in the measured variables X_i.

A very useful specific form can be obtained when the data reduction equation Eq. 3-7 has the form:

$$r = kX_1^a X_2^b X_3^c \cdots \quad , \qquad \text{Eq. 3-9}$$

where the exponents may be positive or n egative constants and k is a con stant. Application of Eq. 3-8 to the relationship of Eq. 3-9 yields:

$$\left(\frac{u_r}{r}\right)^2 = a^2\left(\frac{u_{X_1}}{X_1}\right)^2 + b^2\left(\frac{u_{X_2}}{X_2}\right)^2 + c^2\left(\frac{u_{X_3}}{X_3}\right)^2 + \cdots \quad , \qquad \text{Eq. 3-10}$$

Therefore, use Eq. 3-6 to calculate CTE uncertainty and then Eq. 3-10 yields:

$$\left[u\{\alpha\}\right]^2 = \left[u\left\{\frac{d\times\Delta H}{(2L)\times P\times(T_2-T_1)}\right\}\right]^2 \qquad \text{Eq.3-11}$$

$$= \left[\frac{d\times\Delta H}{(2L)\times P\times(T_2-T_1)}\right]^2 \times \left[\left(\frac{u\{d\}}{d}\right)^2 + \left(\frac{u\{\Delta H\}}{\Delta H}\right)^2 + \left(\frac{u\{2L\}}{2L}\right)^2 + \left(\frac{u\{P\}}{P}\right)^2 + \left(\frac{u\{T_2-T_1\}}{T_2-T_1}\right)^2\right]$$

$$= \alpha^2 \times \left[\left(\frac{u\{d\}}{d}\right)^2 + \left(\frac{u\{\Delta H\}}{\Delta H}\right)^2 + \left(\frac{2u\{L\}}{2L}\right)^2 + \left(\frac{u\{P\}}{P}\right)^2 + \left(\frac{u\{T_1\}^2+u\{T_2\}^2}{T_2-T_1}\right)^2\right]$$

Therefore,

$$u\{\alpha\} = \alpha \times \sqrt{\left(\frac{u\{d\}}{d}\right)^2 + \left(\frac{u\{\Delta H\}}{\Delta H}\right)^2 + \left(\frac{u\{L\}}{L}\right)^2 + \left(\frac{u\{P\}}{P}\right)^2 + \left(\frac{u\{T_1\}^2 + u\{T_2\}^2}{T_2 - T_1}\right)^2}$$

Taking the measured data from the aluminum (Phase 1) as an example,

$$u\{\alpha\} = \frac{(1.0\ cm)\times(-102.9\ cm)}{(2\times 779.8\ cm)\times(153.7\ cm)\times(0.0^oC - 19.7^oC)} \times$$

$$\sqrt{\left(\frac{0.1}{1.0}\right)^2 + \left(\frac{0.3}{102.9}\right)^2 + \left(\frac{1.0}{779.8}\right)^2 + \left(\frac{0.3}{153.7}\right)^2 + \left(\frac{0.1^2 + 0.1^2}{19.7 - 0.0}\right)^2}$$

$$= 21.8\times 10^{-6} \times \sqrt{0.1^2 + \left(2.9\times 10^{-3}\right)^2 + \left(1.3\times 10^{-3}\right)^2 + \left(2.0\times 10^{-3}\right)^2 + \left(1.0\times 10^{-3}\right)^2}$$

$$= 2.2\times 10^{-6} \text{ per } ^oC$$

This indicates that the uncertainty due to *random error* for aluminum CTE test (Phase 1) based on SMOL apparatus is $\pm 2.2\times 10^{-6}$ per ^oC. Therefore, the aluminum CTE (Phase 1) result including uncertainty from random error will be equal to $(21.8 \pm 2.2) \times 10^{-6}$ per ^oC.

For CFRE trial 1, 2 and 3, the CTE results including uncertainty from random error are: $(-0.25 \pm 0.03) \times 10^{-6}$ per ^oC, $(-0.24 \pm 0.03) \times 10^{-6}$ per ^oC and $(-0.24 \pm 0.03) \times 10^{-6}$ per ^oC respectively.

In consideration of the error bars which are more than 10% of each measured value, we conclude that the experiments based on SMOL setup result in unacceptably large random errors.

3.5.2 Systematic Errors in the SMOL Tests

Aside from the uncertainty due to random errors, systemic errors must be also considered and evaluated.

Because the sample and the sleeve rest directly on the concrete floor (Figure 3-8) during the tests, when the temperature of the sample and sleeve change, heat flows to and from the concrete floor, causing the concrete to expand and contract. This end effect results in a systematic error in measuring sample's length change, ΔP.

Also, the sample has non-uniform temperature along the length due to this thermal end effect. However, this effect has not been studied in detail.

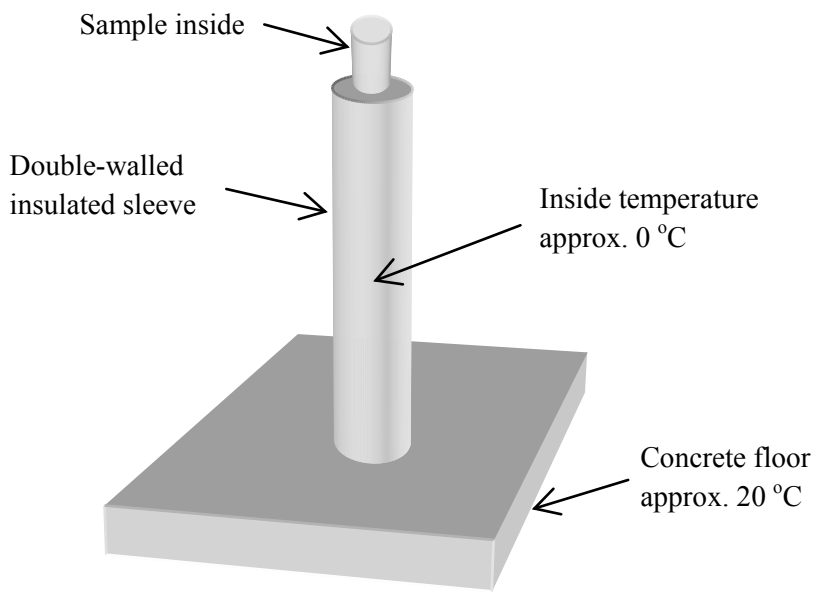

Figure 3-8: SMOL CTE experiment circumstance

To analyze the effect of the expanding concrete floor and correct the results of the first technique, a transient coupled thermo-mechanical finite element analysis using the commercial software ANSYS is conducted to simulate the heat transfer and resulting

floor deformation. The coefficients for ANSYS processing are given in Table 3-3. An axi-symmetric model (shown in Figure 3-9) is created for simplifying the calculation.

Table 3-3. ANSYS parameters used in the analysis

Analysis Model	Parameters	Set Value
Thermal Model	K (Thermal Conductivity)	2.0 W/m·k
	C (Specific Heat Capacity)	750 J/kg·K
	Density of Concrete	2400 kg/m^3
	Initial Temperature	293 K
Structural Model	E (Young's Modulus)	30 GPa
	ν (Poisson's Ratio)	0.2
	CTE of Concrete	12×10^{-6} / K
	Reference Temperature	293 K

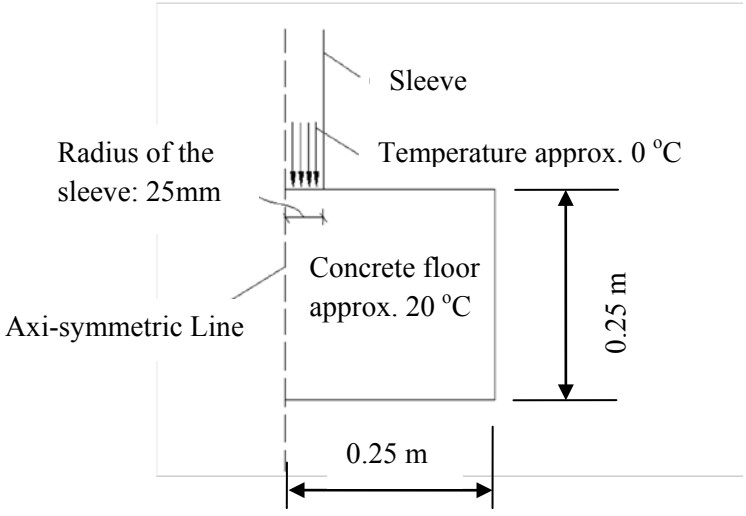

Figure 3-9: Axi-symmetric ANSYS model

In the ANSYS model, a cylindrical concrete area of radius 0.25m and depth 0.25 m is created to simulate the concrete floor, shown in Figure 3-10.

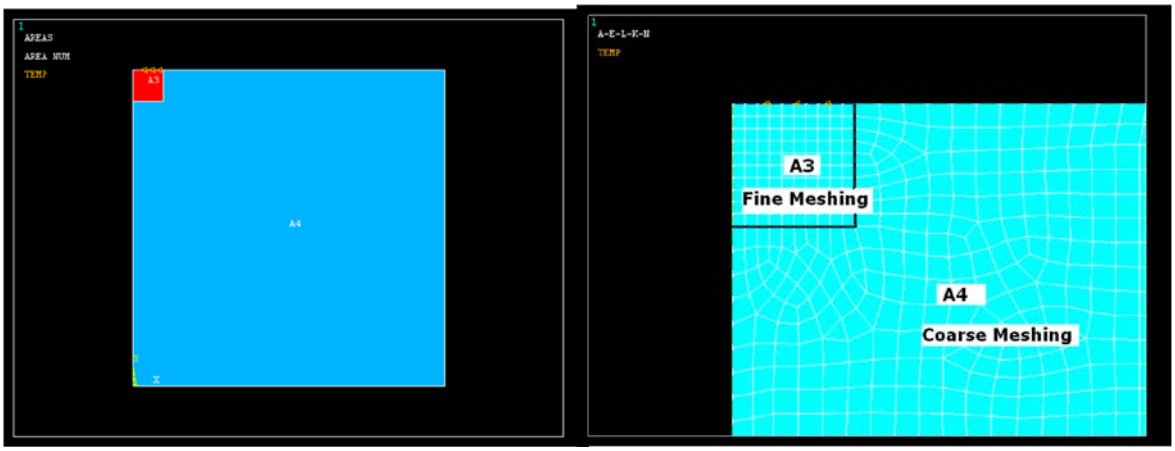

(a) (b)

(a) Entire concrete model

(b) Fine and coarse meshing for different areas

Figure 3-10: Meshing model of concrete floor in ANSYS

In the ANSYS simulation, different physical models such as structural, thermal and magnetic require different element types. Therefore, to apply the ANSYS results from the thermal model to the structural model, it is necessary to build two separate models with different boundary conditions and applied forces. However, because the dimensions and physical conditions are same, the same meshing models are employed directly for the analysis (Figure 3-11).

After these two models are completed, the results can be coupled, shown in Figure 3-12. The temperature result from the thermal model is applied to the structural model to determine the deformation of the concrete floor. In this coupled field analysis,

the time history is also included to obtain the thermal and deformation results as a function of time. Therefore the temperature and deformation values at any specific location and time can be computed.

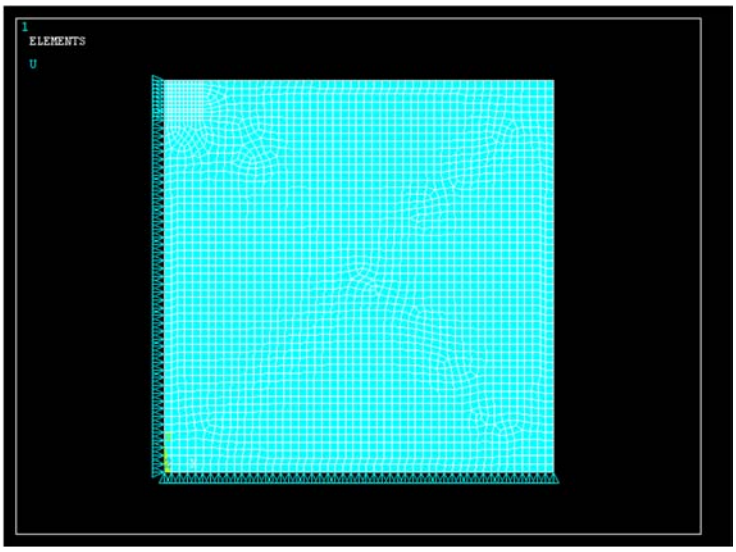

Figure 3-11: Structural model in ANSYS (having the same mesh as the thermal model, but different element type, coefficients, boundary conditions and loads)

In this ANSYS model, the cylindrical concrete area of radius 0.25m and depth 0.25 m (Figure 3-12 (a) and (b)) is sufficiently large for accurate analysis. In a relatively larger model, the result is similar but more time consuming to compute. At any given time, thermal result from Figure 3-12 (a) is applied to the structural model to determine concrete's deformation, shown in Figure 3-12 (b).

Finally, convergence study was conducted, as shown in Table 3-4.

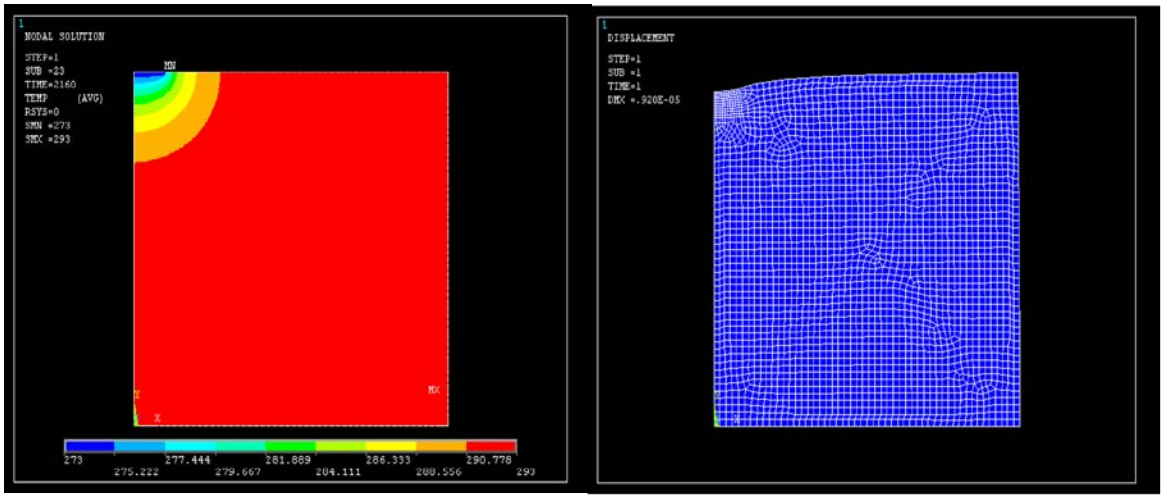

(a) (b)

(a) Temperature result at 2160 seconds (36 min) in SMOL tests

(b) Structural deformation based on temperature result at the same time

Figure 3-12. Finite element method for thermal and structural analysis

Table 3-4. Convergence study of finite element analysis

Number of Elements	Concrete's Deformation (10^{-6}) m
107	9.94
710	9.41
2711	9.20
5990	9.13
10567	9.09

After 36 minutes (experiment duration) and a 20.0 ^{o}C temperature change, the deformation of floor is 9.09×10^{-6} m which implies a CTE error due to $\Delta_{concrete\ floor.}$

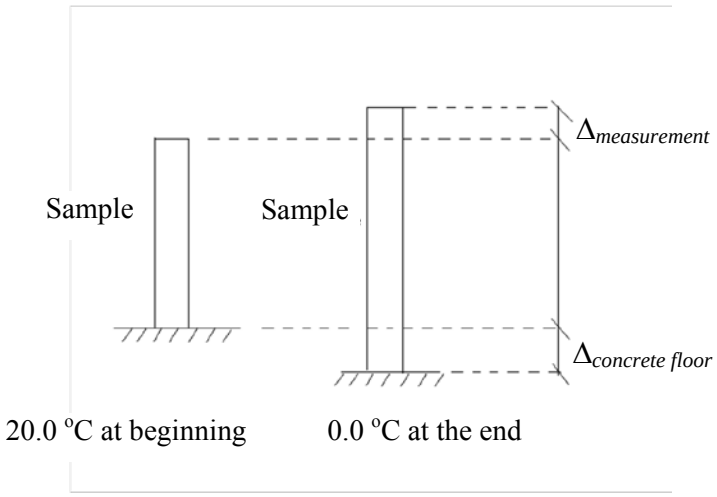

Figure 3-13. Considering $\Delta_{concrete\ floor}$ in systemic errors

As shown in Figure 3-13.

$\Delta_{actual} = \Delta_{concrete\ floor} + \Delta_{measurement}$ (Take data from IM7 CFRE trial 2 as an example)

$\Delta_{actual} = 0.91\times10^{-5}$ m + 0.76×10^{-5} m

$\Delta_{actual} = 1.67\times10^{-5}$ m

According to Eq.3-5, CTE of IM7 CFRE in trial 2 is:

$$\alpha = \frac{\Delta P}{P(T_2 - T_1)} = \frac{1.67\times10^{-5}\,m}{153.7\times10^{-2}\,m\times20^{o}C} = -0.54\times10^{-6}\,per^{o}C \quad ,$$

Including the error bar due to the random errors, the CTE of IM7 CFRE in trial 2 is: α = - (0.54 ±0.03) $\times10^{-6}$ per °C.

Table 3-5 shows the SMOL CTE results including both random and systematic errors. However, it also indicates that the correction for systematic errors in IM7 CFRE tests is on the order of the quantity to be measured. Therefore the tests based on SMOL

method are insufficiently accurate. It is necessary to develop a more accurate and reliable method.

Table 3-5: Aluminum, steel and IM7 CFRE CTE results based on SMOL tests (including both random and systematic errors)

Sample	CTE (under 100°C) from literature [30, 31] Per C×10^{-6}	CTE of Phase 1 Per C×10^{-6}	CTE of Phase 2 Per C×10^{-6}	CTE, average of Phases 1&2 Per C×10^{-6}
Aluminum	23 ~ 24	21.5 ± 2.2	20.9 ± 2.1	21.2 ± 2.2
Stainless Steel	16.9 ~17.3	15.6 ± 1.6	15.0 ± 1.5	15.3 ± 1.6
IM7 CFRE trial 1	- 0.64 (From Hexcel technical data sheets)	- (0.55 ± 0.03)	- (0.55 ± 0.03)	- (0.55 ± 0.03)
IM7 CFRE trial 2		- (0.53 ± 0.02)	- (0.55 ± 0.03)	- (0.54 ± 0.03)
IM7 CFRE trial 3		- (0.53 ± 0.02)	- (0.55 ± 0.03)	- (0.54 ± 0.03)

3.6 Discussion

In this chapter, using a classical optical lever experiment, a single-mirror optical lever (SMOL) is introduced for measuring CTE of aluminum, stainless steel and IM7 CFRE. There is only one single spot produced by the laser pointer, and therefore care must be taken during the test to avoid disturbing the laser pointer. As one part of the error analysis, uncertainty due to random errors in SMOL tests is considered in Section 3.5.1. The error bars are provided for each measured CTE value.

The other problem existing in the SMOL setup is: the whole temperature of the sample is controlled by circulating cold/warm water. However, the sample's temperature would be inevitably influenced by heat conduction from the ends. Section 3.5.2 focused

on discussing systematic errors during the test. Finally, it turns out that the correction for systematic errors in the SMOL apparatus is 0.91×10^{-5} m. Also, this correction for systematic errors is even larger than the measured deformation of IM7 CFRE, which is 0.76×10^{-5} m.

Although this SMOL setup has been shown to be a possible method for measuring the ultra low CTE of IM7 CFRE material, it does not provide sufficient accuracy considering the high random and systematic errors. Therefore, an improved method is necessary for our research purposes. The next chapter describes an improved experimental technique called DMOL.

Chapter 4

Experiment II: Measurement of Coefficient of Thermal Expansion Using Double-Mirror Optical Lever (DMOL)

4.1 Introduction

In the Chapter 3, a single-mirror optical lever (SMOL) was introduced and used to determine the coefficient of thermal expansion (CTE) of carbon fiber reinforced epoxy (CFRE) composite material.

The SMOL makes use of both a mechanical and an optical lever to measure the length change of a sample. However, random and systematic errors in the SMOL tests (referring to Chapter 3, section 3.5) are unacceptably large compared to the magnitude of the measured values. Additionally, with this method, a small disturbance of the laser location can cause relatively large movement of the spot on the screen. Thus, the position of the laser pointer has to be controlled very precisely during the tests. This shortcoming will be very difficult to eliminate for the coefficient of moisture expansion (CME)

measurement, because the laser pointer has to be turned on and off during the long-duration test.

To better control the device during CTE and CME tests and lower the negative influence from both random and systematic errors, an improved method is necessary for our purposes. In this chapter, an improved optical dilatometer called the double-mirror optical lever (DMOL) is developed, and a temperature-controlled chamber is employed to correct the shortcomings from the previous SMOL technique. Most importantly, a more accurate CTE measurement for IM7 CFRE is developed using the DMOL method.

4.2 Theory and Equations for DMOL

The DMOL is an improvement upon the SMOL. With the DMOL setup shown in Fig. 4-1(b), due to the laser beam reflection between the silvered mirror and the beam splitter, the DMOL setup can produce multiple spots on the screen and consequently provide more precise measurements compared to the single spot in the SMOL setup (Figure 4-1(a)). Also, because the deformation of the sample from the DMOL causes differential spot motion on the screen, small changes in laser location do not cause significant errors in measurement. Finally, because the entire test is enclosed within an environmental chamber, it is of spatially uniform temperature, thus eliminating systematic errors due to thermal gradients. Details of the DMOL geometric relationship are shown in Figure 4-2.

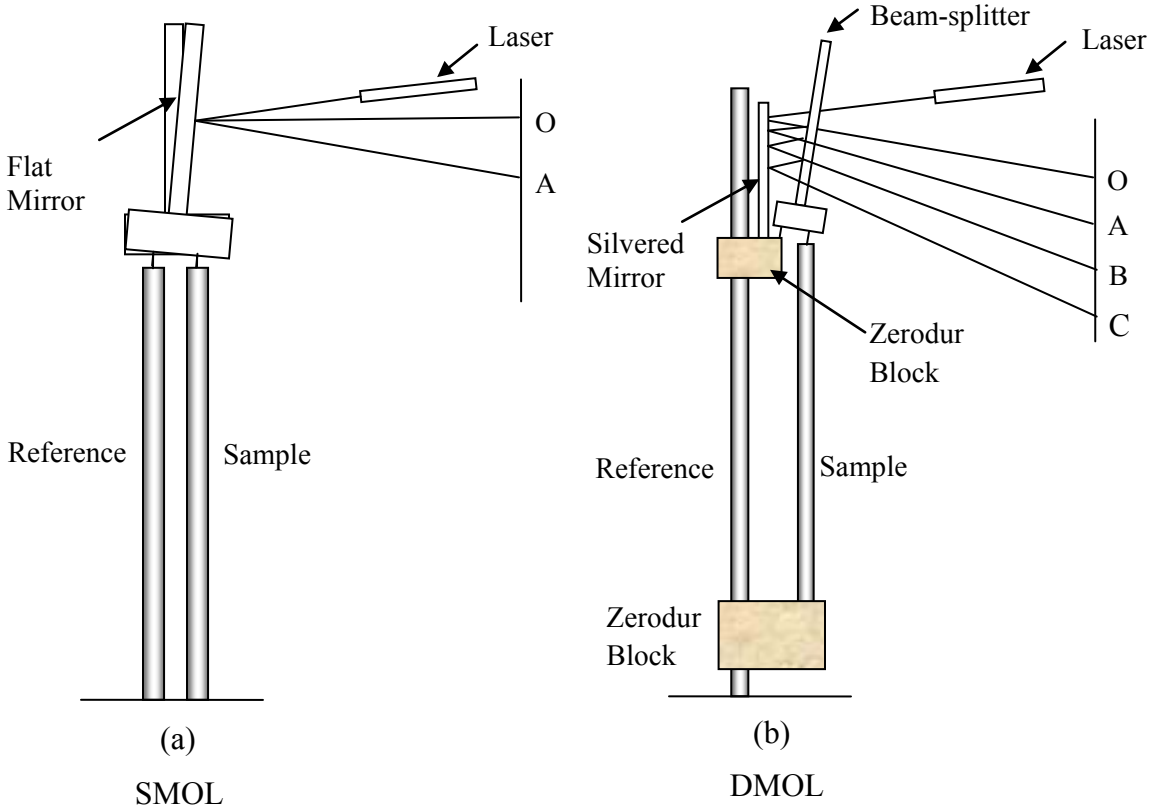

Figure 4-1. Schematic of the SMOL and DMOL methods

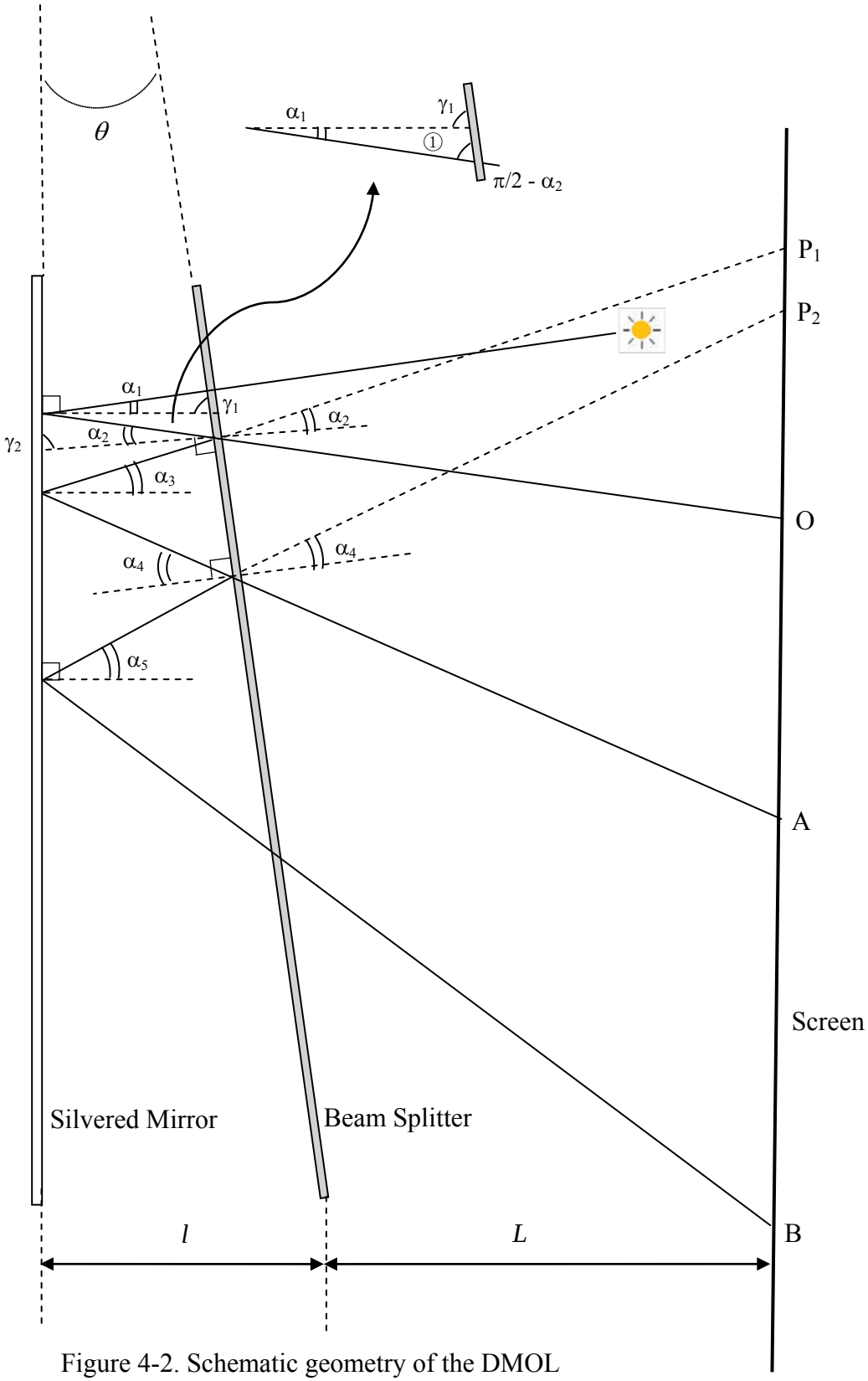

Figure 4-2. Schematic geometry of the DMOL
(Note: $l << L$ *and* $\alpha_i \approx 0^o$. Angles are exaggerated in this figure.)

The definition of the notation used in Figure 4-2 is given in Table 4-1.

Table 4-1. Notation definition of the DMOL

Notation	Definition
α_1	First angle of incidence at surface of silvered mirror
α_2	First angle of incidence at surface of beam splitter
α_3	Second angle of incidence at surface of silvered mirror
α_4	Second angle of incidence at surface of beam splitter
α_5	Third angle of incidence at surface of silvered mirror
θ	The angle between silvered mirror and beam splitter
γ_1	The angle between beam splitter and normal of silvered mirror
γ_2	The angle between silvered mirror and normal of beam splitter
l	The horizontal distance between the bottoms of silvered mirror and beam splitter
L	The horizontal distance between the bottoms of beam splitter and screen

Based on Figure 4-2, the following equations are derived.

Because the sum of the angles in a triangle is equal to π,

$\theta + \gamma_1 + \frac{\pi}{2} = \pi$, and in the triangle ①: $\gamma_1 = \alpha_1 + (\frac{\pi}{2} - \alpha_2)$,

Eliminating γ_1 in the above two equations, $\Rightarrow \theta + \alpha_1 = \alpha_2$

By the same reasoning, in general, $\theta + \alpha_i = \alpha_{i+1}$

Therefore, $n \cdot \theta + \alpha_1 = \alpha_{n+1}$ Eq. 4-1

For the triangles that contain α_2 and α_3, because α_2 and α_3 are small enough (as long as $-6^o < \alpha_i < 6^o$), using the small angle approximation:

$$\theta + \alpha_1 = \alpha_2 = \frac{P_1 O}{2L}, \text{ and}$$

$$2\theta + \alpha_1 = \alpha_3 = \frac{P_1 A}{2(L+l)},$$

which yields, $2\theta L + 4\theta l + 2\alpha_1 l = OA$. Eq. 4-2

When the beam splitter tilts by Δθ, $\Delta\theta = \theta - \theta'$.

For the new spots' position, the new relationship is:

$2\theta' L + 4\theta' l + 2\alpha_1 l = OA'$. Eq. 4-3

Thus, Eq. 4-2 - Eq. 4-3 yields:

$$\Delta\theta = \frac{OA - OA'}{2L + 4l} = \frac{OA - OA'}{2L} = \frac{\Delta A}{2L}.$$ Eq. 4-4

For triangles that contain α_4 and α_5, using the same process, we have:

$2\theta L + 8\theta l + 2\alpha_1 l = AB$, and Eq. 4-5

$$\Delta\theta = \frac{OB - OB'}{4L} = \frac{\Delta B}{4L}.$$ Eq. 4-6

Therefore, in general, $\Delta\theta = \frac{OE - OE'}{(2n)L}$ Eq. 4-7

Eq.4-7 indicates that when there is rotation Δθ of beam splitter, the movement of the point B is as twice the movement of point A. If we assume point A has unit distance δ, namely $\Delta A = \delta$, during the rotation Δθ, the movement of each point would be: $\Delta B = 2\delta$, $\Delta C = 3\delta$, $\Delta D = 4\delta$, $\Delta E = 5\delta$ and so on (Figure 4-3). Therefore, compared to the SMOL setup which only provides the movement ΔA of the single spot A, the improved DMOL setup is producing multiple spots with higher magnification and thus higher resolution.

Another important advantage found in this DMOL setup is: when the laser pointer is moved slightly, it will result in a certain small angle change to α_1, according to Eq.4-2 and Eq. 4-5, because $2\alpha_1 l$ is much smaller compared to other terms, OA and AB will be approximately as same as before. For instance, if α_1 is changed to α_1' in the test, OA, AB, BC, CD and DE will still keep the same length but will have a shift on the screen. Therefore, because what we measure is the distance between spots, measurement errors due to small laser position disturbances can be neglected. This advantage is beneficial to the repeatability and reliability of the DMOL setup.

To better demonstrate the relationship of the displacement of each point during the test, two photographs, Figure 4-3 (a) and (b), taken from two different times are presented and aligned for comparison.

As shown in Figure 4-3, an array of spots is produced and can be clearly observed on the screen.

The first point A in DMOL setup is the equivalent to the single point in the SMOL setup. According to Eq. 3-6 in Chapter 3, the CTE of the measured sample based on the SMOL setup is equal to

$$\alpha = \frac{d}{(2L)\times P\times (T_2 - T_1)} \times \Delta A\,, \qquad \text{Eq.4-8}$$

where, ΔA substitutes for ΔH.

Because the value of OE - O'E' is as five times the value of OA - O'A', we have OE - O'E' = 5×(OA - O'A'). Therefore, point E in the DMOL setup has the CTE equation as follows.

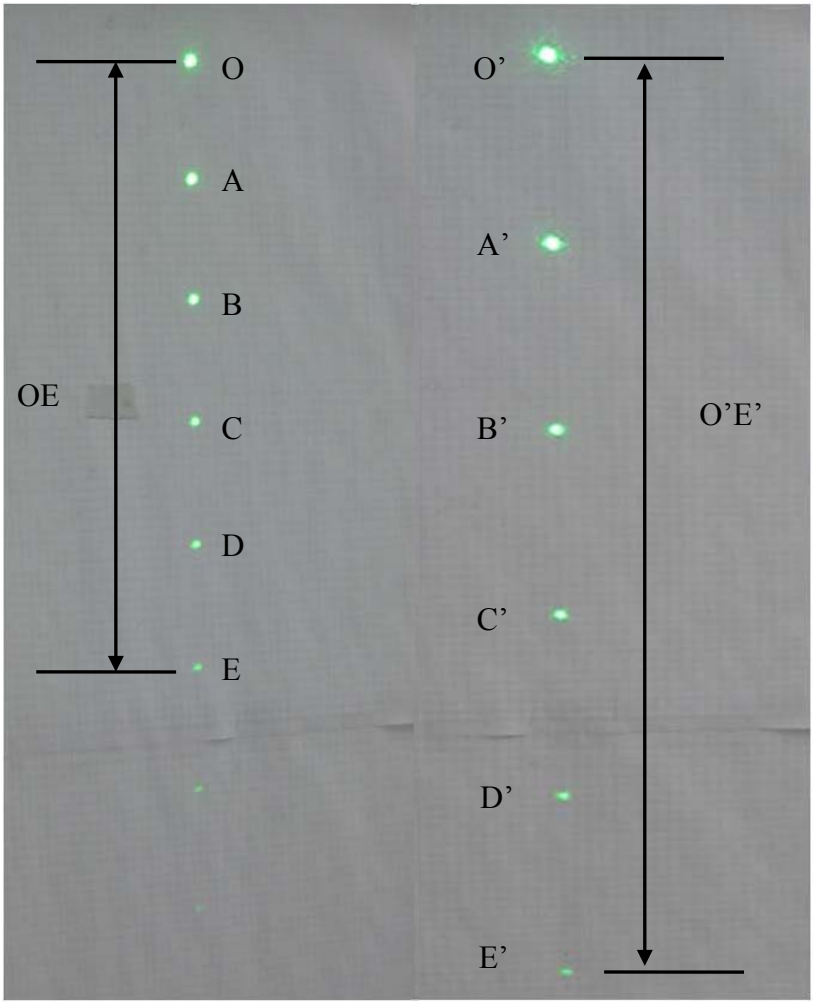

(a) (b)

Figure 4-3. Spots’ movements in the DMOL CTE test

$$\alpha = \frac{d}{(2L)\times P\times (T_2 - T_1)} \times \frac{O'E' - OE}{5}, \qquad \text{Eq.4-9}$$

where, $O'E' - OE = \Delta E$,

and, $\Delta H = \frac{O'A' - OA}{1} = \frac{O'B' - OB}{2} = \frac{O'C' - OC}{3} = \frac{O'D' - OD}{4} = \frac{O'E' - OE}{5}$.

Eq. 4-9 is used for calculating the CTE of IM7 CFRE in the DMOL test. More details are provided in Section 4.7 in this chapter.

4.3 Devices and Setup for the DMOL Method

The whole experimental setup is placed in an environmental chamber which controls the temperature with a tolerance of ±0.5 ^{o}C. The DMOL experiment setup presented in the previous section is shown in Figure 4-4 with more details. Zerodur and quartz rod are used because of their ultra-low CTE. Figure 4-5 shows the interior and exterior of the environmental chamber.

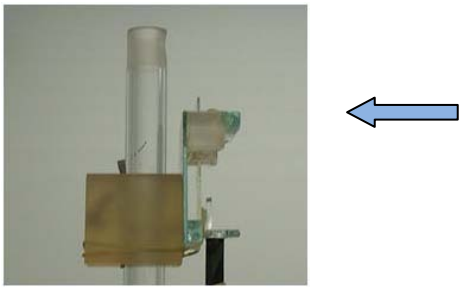

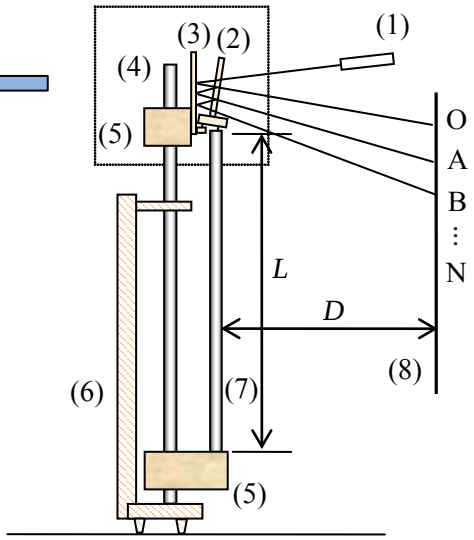

1. Laser Pointer
2. Beam-Splitter
3. Silvered Mirror
4. Quartz Rod (Reference)
5. Zerodur Blocks
6. Stand
7. Sample
8. Screen

Figure 4-4. Schematic of the DMOL setup

(a)

(b)

(c)

(a). Interior of environmental chamber showing metering rod setup

(b). Electronic thermometer for measuring the inside temperature

(c). Exterior of environmental chamber showing temperature-controlled panel

Figure 4-5. Photos of environmental chamber

4.4 Operating Procedure for the DMOL Method

The operating procedure for measuring CTE using DMOL method is described as follows:

(1) The sample is placed in the DMOL setup with the bottom end resting on the Zerodur block and the top end contacting one footing of the mirror lever. Care must be taken to assure good seating of the sample.

(2) Three electronic thermometers are kept at three levels (high, medium and low) to measure the thermal gradient in the sample due to chamber convection currents.

(3) The chamber temperature is changed using the control panel. Similar to the SMOL test, the temperature changes have two phases: Phase-1 represents temperature decreasing and Phase-2 represents temperature increasing. For instance, for the CTE measurement of steel and aluminum, it is changed from approximately 20 ^{o}C to approximately 18 ^{o}C and then from approximately 18 ^{o}C to approximately 20 ^{o}C. (Note: the range of temperature change guarantees that the movement of the spot is observable and does not exceed the range of the screen). For the IM7 CFRE test, the temperature range is larger due to its ultra low CTE.

(4) The laser pointer is activated when the test begins. The DMOL setup is adjusted to project the laser spots as clearly and centrally as possible on the screen.

(5) Photographs are taken of both the spots' position on the screen and the electronic thermometers' readings during the test. Copy spots position to another identical screen, and then measure the distance between each spot. The CTE of the sample is calculated based upon the distance change (for instance, $\Delta E = OE - O'E'$) and also based upon the temperature change.

4.5 Temperature Study of the Environmental Chamber

To accurately determine the CTE of the metering rod, it is necessary to know the temperature quite precisely. Figure 4-6 shows the measured air temperatures in the environmental chamber using a very precise mercury thermometer placed at mid-height in the chamber (MT-Med), three electronic thermometers placed near the metering rod at low, medium, and high positions within the chamber (ET-Low, ET-Med, ET-High), and the temperature recorded on the front panel of the chamber (PT).

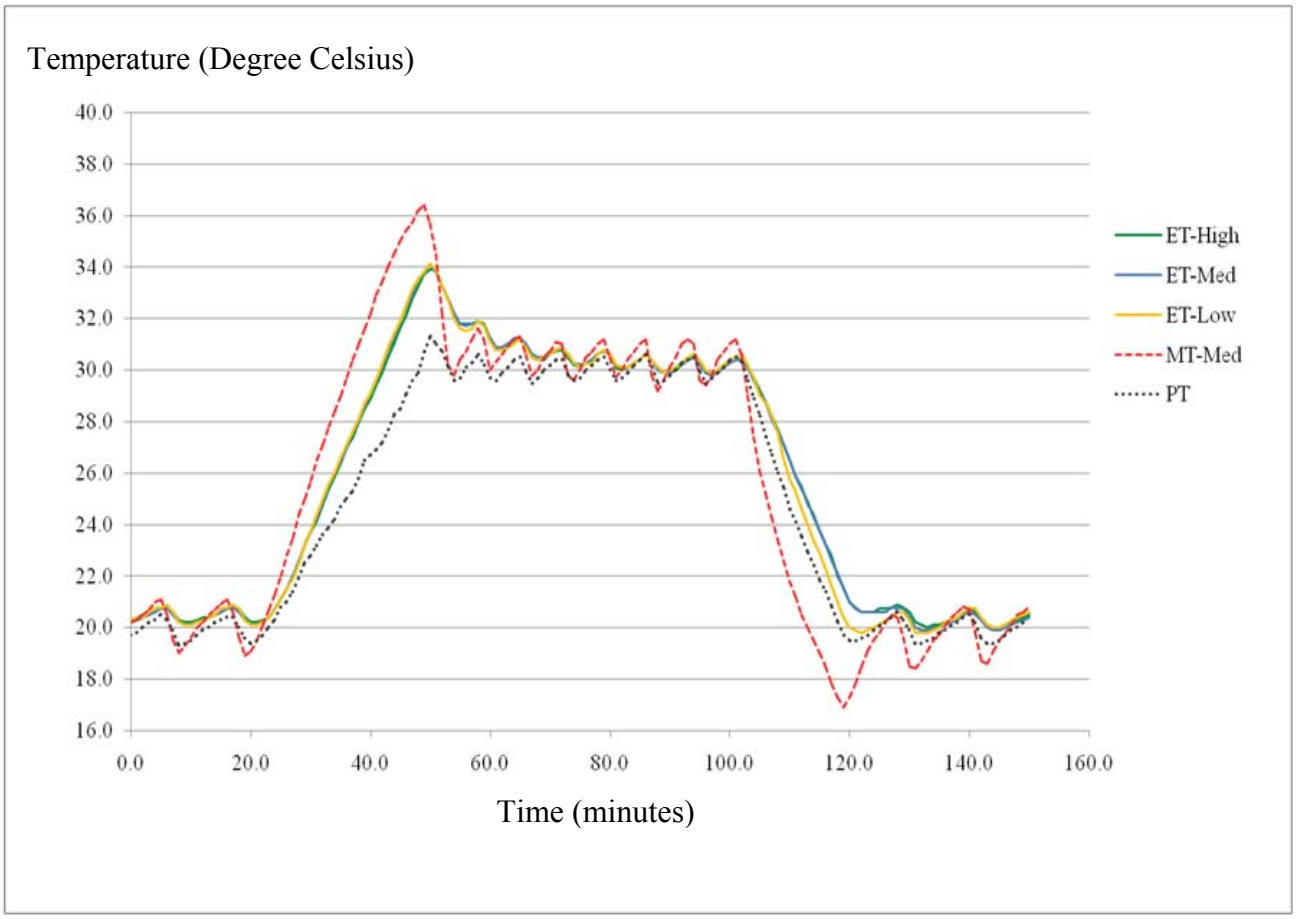

Figure 4-6. Measured temperature using various thermometers

The temperature in the environmental chamber is controlled by a thermostatically-controlled cooler. During the process, the heater is on all the time, and the cooler is switched on when the temperature measured by the thermostat is below the control range, which has a tolerance of ± 0.5 ^{o}C. For instance, when the set temperature equals 20.0 ^{o}C, the panel temperature (PT) varies between 19.5 ^{o}C and 20.5 ^{o}C. When the PT is in this range, the heater is on and the cooler is off. Thus, the temperature keeps rising slowly during this phase. Whenever the PT exceeds 20.5 ^{o}C, the cooler is switches on while the heater is still on. But due to the efficiency of the cooler, the temperature drops more quickly than it rises.

Figure 4-6 indicates that the temperature measured by the electronic thermometers is different from panel temperature. During the temperature cycling, the difference between them is as high as 3 ^{o}C, but when the chamber is in thermal equilibrium, the difference is only approximately 0.3 ^{o}C.

A very accurate calibrated mercury thermometer has been employed to calibrate the electronic thermometers. This mercury thermometer is placed at medium level next to one of the electronic thermometers. Figure 4-6 also shows that the mercury thermometer gives a wider temperature range than the other thermometers due to its thermal responsiveness.

As shown in Figure 4-6, it is clear that during steady-state operation, the air temperature varies by about one degree Celsius with a cyclic frequency of approximately 5 minutes. Therefore, the metering rod would be expected to respond with milder temperature swings compared to the electronic thermometer. With these temperature swings, it is reasonable to assume that the temperature of the sample is approximately

equal to the average of three electronic thermometer values. This information is essential in determining the temperature variations in the metering rod and sample, because in the following CTE calculation the sample's temperature is assumed as the average value from the three electronic thermometers. For instance, the temperature values T_1 and T_2 in Table 4-3 are obtained by averaging the values of temperature from these three electronic thermometers.

4.6 Optical Levers used in the DMOL Setup

In the DMOL experimental setup, two Optical Levers (I and II) shown in Figure 4-7 were used independently for measuring CTE. The main difference of these two optical levers is the length of d, which is the distance between two footings of the beam splitter (see Figures 4-4 and 4-7). Because d is very small (less than 1 cm) and most importantly, its accuracy with which it is measured directly affects with the whole measuring accuracy of CTE, a dial caliper with high accuracy (±0.001 in) is employed for determining d.

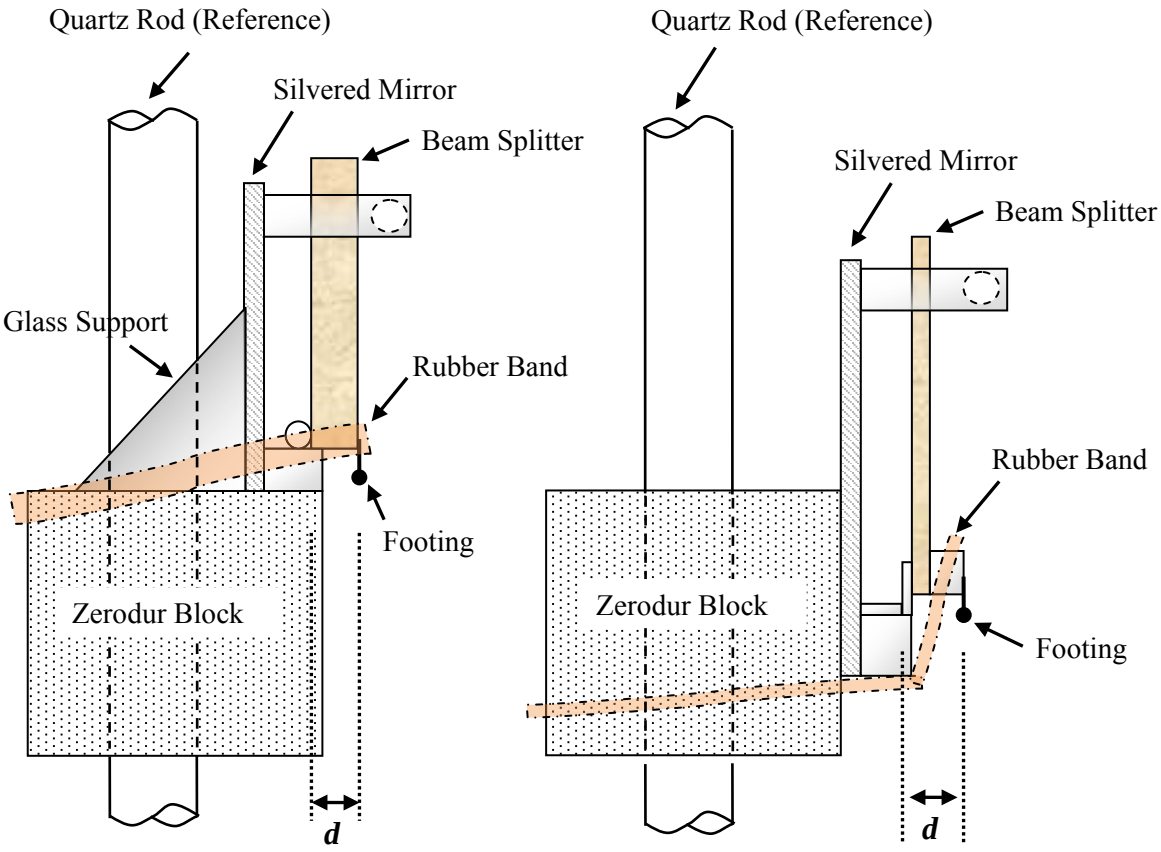

Figure 4-7. Schematic of Optical Levers I and II

Optical Lever-I was first developed, shown in Figure 4-8.

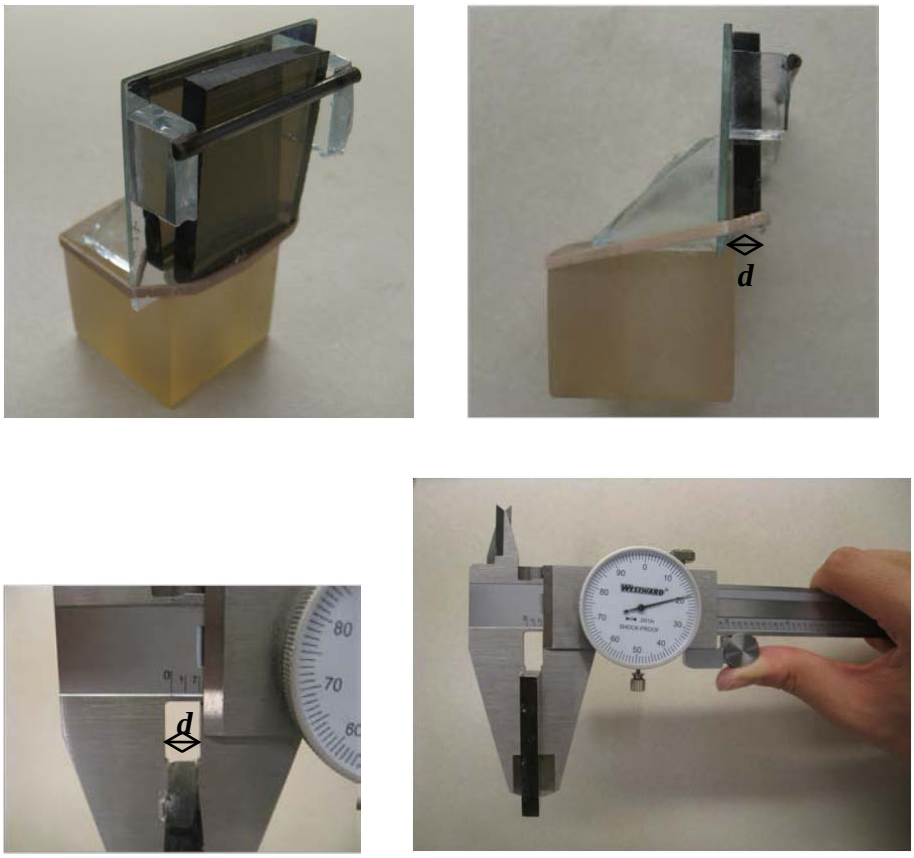

Figure 4-8. Measurement of *d* of Optical Lever-I using a dial caliper

Optical Lever-II, shown in Figure 4-9 is an improvement compared to Optical Lever-I in terms of higher magnification of the movement of the laser spots on the screen, high quality beam splitter and better fabrication.

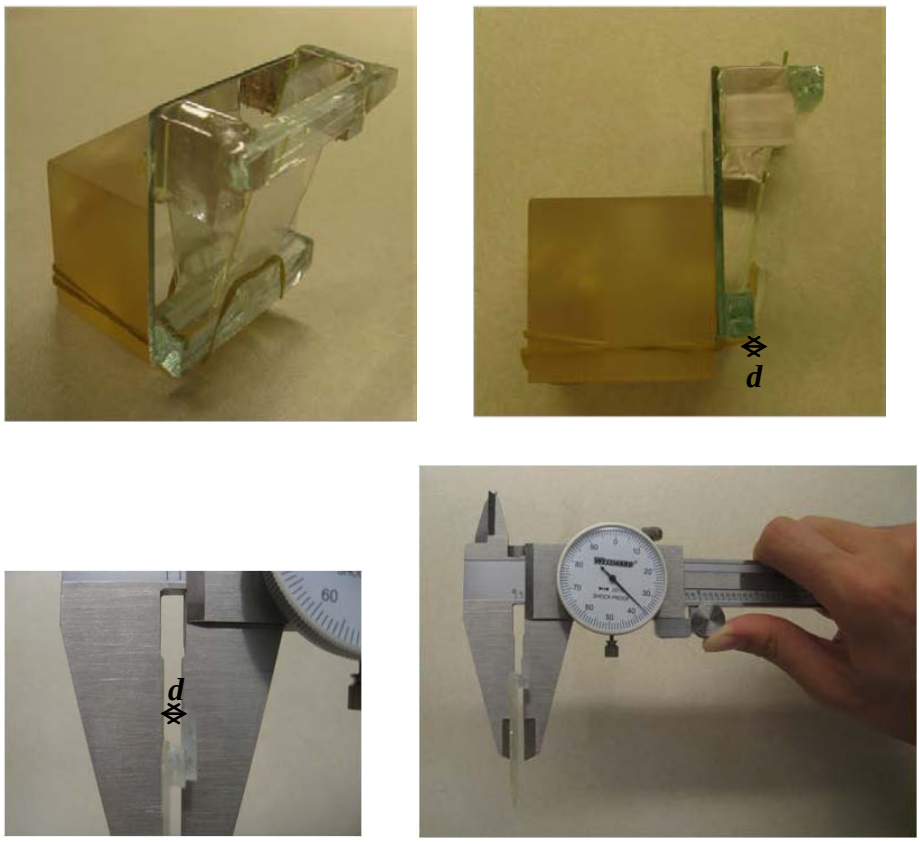

Figure 4-9. Measurement of *d* of Optical Lever-II using dial caliper

The measuring results for the two different optical levers are shown in Table 4-2. Because Optical Lever-II has the smaller *d*, it provides higher magnification. In the following CTE tests of aluminum, stainless steel and IM7 CFRE, both Optical Lever-I and Optical Lever-II are used to verify the reliability and repeatability of the DMOL method.

Table 4-2. Measured values of *d* in Optical Lever-I and -II

Type	*d* (cm)	Uncertainty (cm)	Normalized Magnification (assume Optical Lever-I as 1)
Optical Lever-I	0.219 in ≈ 0.556 cm	0.001 in ≈ 0.00254 cm	1
Optical Lever-II	0.138 in ≈ 0.351 cm	0.001 in ≈ 0.00254 cm	$\frac{0.556}{0.351} = 1.58$

4.7 CTE Experimental Results using the DMOL Method

The CTE calculation using the DMOL method is based on Eq.4-9. Measured data are listed in Table 4-3.

Table 4-3. Measured CTE values using DMOL
(without considering random and systematic errors)

Type	Sample	d cm	ΔH cm	L cm	P cm	T_1 Per °C	T_2 Per °C	α Per °C $\times 10^{-6}$
Optical Lever I	Stainless Steel (Phase 1)	0.556	-6.27	350.8	153.7	20.3	18.4	17.01
	Stainless Steel (Phase 2)	0.556	6.67	350.8	153.7	18.0	20.0	17.19
Optical Lever I	Aluminum (Phase 1)	0.556	-9.43	350.8	153.7	20.2	18.1	23.16
	Aluminum (Phase 2)	0.556	9.60	350.8	153.7	18.0	20.1	23.57
Optical Lever II	Aluminum (Phase 1)	0.351	-15.33	350.8	153.7	22.4	20.3	23.77
	Aluminum (Phase 2)	0.351	14.43	350.8	153.7	20.2	22.2	23.49
Optical Lever I	IM7 CFRE (Phase 1)	0.556	0.83	461.2	153.7	20.1	16.0	-0.784
	IM7 CFRE (Phase 2)	0.556	-0.76	461.2	153.7	16.2	20.2	-0.745
Optical Lever II	IM7 CFRE (Phase 1)	0.351	-3.04	461.2	153.7	20.2	30.2	-0.753
	IM7 CFRE (Phase 2)	0.351	-3.12	461.2	153.7	20.2	30.3	-0.765
	IM7 CFRE (Phase 3)	0.351	-3.22	461.2	153.7	20.2	30.1	-0.805
	IM7 CFRE (Phase 4)	0.351	-3.26	461.2	153.7	20.2	30.1	-0.815

In Table 4-3:

(1) Stainless steel samples are measured only using Optical Lever I. Phase 1 represents temperature decrease and Phase 2 represents the temperature increase;

(2) Aluminum samples are measured using both Optical Lever I and II. Phase 1 represents temperature decrease and Phase 2 represents the temperature increase;

(3) IM7 CFRE samples are measured using both Optical Lever I and II. Differently, Phase 1 ~ Phase 4 respectively represent CTE measurements at four different durations for one single continuous test (test durations are available in Table 4-7).

Table 4-3 provides the new CTE results using the DMOL method. However, random and systematic errors are known to exist. The error evaluation process for the DMOL method is as follows.

4.7.1 Random errors in the DMOL tests

The process for evaluating the SMOL's uncertainty due to the random error is demonstrated in Chapter 3, Section 3.5.1. Similarly, uncertainty propagation is applied in DMOL's uncertainty calculation. As in Section 3.5.1, one CTE test is taken as the calculation example. "Stainless Steel (Phase 1)" from CTE results Table 4-3 is used in Table 4-4 for obtaining the uncertainty.

Table 4-4. Measured values in stainless steel CTE test (Phase 1) with their estimated uncertainties

Notation	Definition	Measured Value	Estimated Uncertainties
α	Coefficient of Thermal Expansion	／	／
d	Distance between two mirror footings	0.556 cm	± 0.00254 cm
OC	Distance between O and C	54.2 cm	± 0.3 cm
O'C'	Distance between O' and C'	35.4 cm	± 0.3 cm
L	Distance between the beam-splitter and screen (see Figure 4-2)	350.8 cm	± 1.0 cm
P	Sample's original length	153.7 cm	± 0.3 cm
T_1	Temperature at beginning	20.3 °C	± 0.1 °C
T_2	Temperature at ending	18.4 °C	± 0.1 °C

According to Eq.4-8, the CTE calculation in the DMOL is:

$$\alpha = \frac{d}{(2L)\times P\times(T_2 - T_1)}\cdot\frac{O'C'-OC}{3} \quad ,$$

Therefore, using the same process (Chapter 3, Section 3.5 and Eq. 3-11) for uncertainty propagation calculation:

$$[u\{\alpha\}]^2 = \left[u\left\{ \frac{d}{(2L)\times P\times(T_2 - T_1)}\cdot\frac{O'C'-OC}{3} \right\} \right]^2$$

$$= \left[\frac{d}{(2L)\times P\times(T_2 - T_1)}\cdot\frac{O'C'-OC}{3} \right]^2 \times$$

$$\left[\left(\frac{u\{d\}}{d}\right)^2 + \left(\frac{\frac{1}{3}\cdot u\{O'C'-OC\}}{\frac{1}{3}\cdot(O'C'-OC)}\right)^2 + \left(\frac{u\{2L\}}{2L}\right)^2 + \left(\frac{u\{P\}}{P}\right)^2 + \left(\frac{u\{T_2-T_1\}}{T_2-T_1}\right)^2 \right]$$

$$= \alpha^2 \times \left[\left(\frac{u\{d\}}{d}\right)^2 + \left(\frac{u\{O'C'\}^2+u\{OC\}^2}{O'C'-OC}\right)^2 + \left(\frac{2u\{L\}}{2L}\right)^2 + \left(\frac{u\{P\}}{P}\right)^2 + \left(\frac{u\{T_1\}^2+u\{T_2\}^2}{T_2-T_1}\right)^2 \right],$$

which yields,

$$u\{\alpha\} =$$

$$\alpha \times \sqrt{\left(\frac{u\{d\}}{d}\right)^2 + \left(\frac{u\{O'C'\}^2+u\{OC\}^2}{O'C'-OC}\right)^2 + \left(\frac{u\{L\}}{L}\right)^2 + \left(\frac{u\{P\}}{P}\right)^2 + \left(\frac{u\{T_1\}^2+u\{T_2\}^2}{T_2-T_1}\right)^2}\ .$$

Taking the data from stainless steel (Phase 1) CTE test in Table 4-3 as an example,

$$u\{\alpha\} = \frac{(0.556)}{(2\times 350.8)\times(153.7)\times(18.4-20.3)}\cdot\frac{35.4-54.2}{3}\ \times$$

$$\sqrt{\left(\frac{0.00254}{0.556}\right)^2 + \left(\frac{0.3^2+0.3^2}{35.4-54.2}\right)^2 + \left(\frac{1.0}{350.8}\right)^2 + \left(\frac{0.3}{153.7}\right)^2 + \left(\frac{0.1^2+0.1^2}{20.3-18.4}\right)^2}$$

$$= 17.01\times 10^{-6} \times \sqrt{(4.57\times 10^{-3})^2 + (9.57\times 10^{-3})^2 + (2.85\times 10^{-3})^2 + (1.95\times 10^{-3})^2 + (0.011)^2}$$

$$= 0.26 \times 10^{-6}$$

Therefore, for stainless steel (Phase 1), CTE = (17.01 ± 0.26) $\times 10^{-6}$ per ^{o}C

Table 4-5 shows the DMOL CTE results considering random errors but without systematic errors.

Table 4-5. CTE results of aluminum, stainless steel and IM7 CFRE using the DMOL method and Optical Lever I and II (Including random errors, but without systematic errors)

Sample	CTE (under 100°C) from literature [30, 31] Per C $\times 10^{-6}$	Average CTE using Optical Lever I Per C $\times 10^{-6}$	Average CTE using Optical Lever II Per C $\times 10^{-6}$
Aluminum	23~24	23.37±0.30	23.63 ± 0.32
Stainless Steel	16.9~17.3	17.10±0.26	/
IM7 CFRE	- 0.64 (From Hexcel technical data sheets)	-0.755±0.036	-0.784±0.011

4.7.2 Systematic errors in the DMOL tests

Because a fused quartz (amorphous silica) rod is used as the reference standard, the CTE measurement of the sample needs to account for the deformation of this fused quartz reference. The CTE of our fused silica meter rod is not precisely known. The reported literature values of the CTE of fused quartz vary between 0.40×10^{-6} per °C and 0.56×10^{-6} per °C at room temperature (0~30 °C) [36, 37, 38]. However, we can consider the DMOL apparatus has an inherent overall CTE which includes the CTE of the fused quartz reference. As for the Zerodur blocks which are supporting the test sample (shown in Figure 4-4), they have no influence due to Zerodur's low-CTE almost null and their small dimension in the DMOL setup.

To determine this overall CTE value of the apparatus (or systematic errors in the DMOL), a Zerodur rod is purchased and employed as a test sample. This Zerodur piece is

a low-CTE glass produced solely by Schott, AG, and has a guaranteed CTE of $0 \pm 0.001 \times 10^{-6}$ per ^{o}C in the temperature range from 0 ^{o}C to 50 ^{o}C.

Similar to the previous DMOL test for aluminum, stainless steel and IM7 CFRE, the Zerodur rod sample is placed in the DMOL setup (Figure 4-10(a)). The bottom end rests on the Zerodur block and the top end supports one foot of the optical lever (Figure 4-10(b)). To laterally secure the sample, a suitable support is used below the Zerodur block.

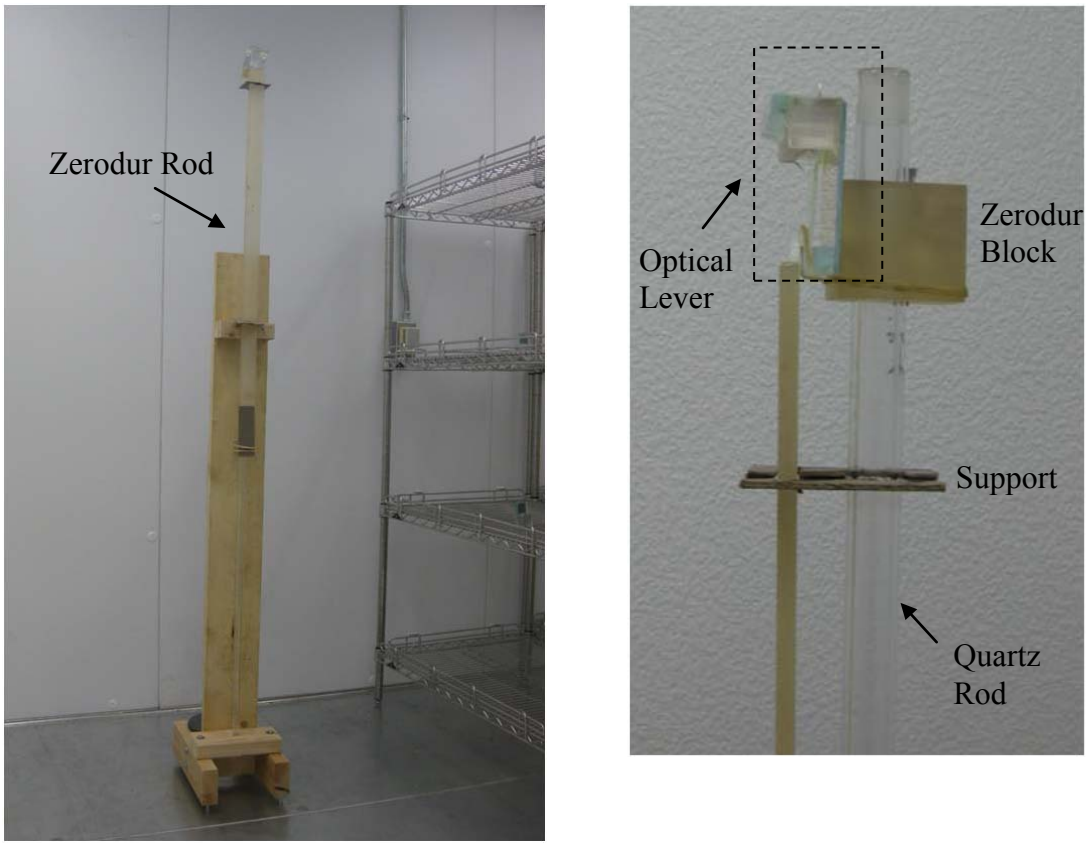

(a) (b)

(a). Using Zerodur as the sample in the DMOL apparatus
(b). Side view of the DMOL apparatus

Figure 4-10. Photos of CTE measurement of DMOL apparatus

Because the purchased Zerodur rod has a known CTE, it is possible to use this Zerodur rod for determining the DMOL apparatus' CTE. Four group tests are conducted to explore the relationship between the DMOL apparatus' CTE and test duration (Table 4-6). Each group includes several tests. Test-1 and Test-2 are conducted within a shorter duration and contain both temperature decreasing and increasing phases. For instance, Test-1 has two tests, one is for temperature increasing from 20.4 ^{o}C to 30.3 ^{o}C; another one is for temperature decreasing from 30.1 ^{o}C to 20.3 ^{o}C. Test-3 and Test-4 are conducted within a longer duration and contain only temperature increasing phases. For instance, Test-3 starts at 20.3 ^{o}C and CTE data are collected periodically until four hours (240 minutes) later.

Finally, Figure 4-11 indicates the relationship between the measured the CTE of DMOL apparatus and test duration.

Table 4-6. The measured overall CTE of the DMOL apparatus (or systematic error) using Zerodur as sample (in sequence of test duration)

Name	Temperature Change (^{o}C)	Test Duration (minutes)	Measured DMOL Apparatus' CTE (Per ^{o}C)
Test - 1	20.4-30.3	37	5.30E-08
	30.1-20.3	40	7.00E-08
Test - 2	20.2-30.2	62	1.02E-07
	30.0-20.1	70	1.37E-07
	20.3-30.2	72	1.39E-07
	30.4-20.1	75	1.63E-07
Test - 3	20.3-30.1	100	1.80E-07
	-30.3	120	1.73E-07
	-30.2	140	1.65E-07
	-29.8	180	2.10E-07
	-30.2	240	1.95E-07
Test - 4	20.1-30.2	60	1.21E-07
	-30.3	120	1.55E-07
	-30.0	180	1.77E-07
	-29.7	240	2.20E-07
	-29.9	300	2.02E-07
	-30.3	360	2.15E-07

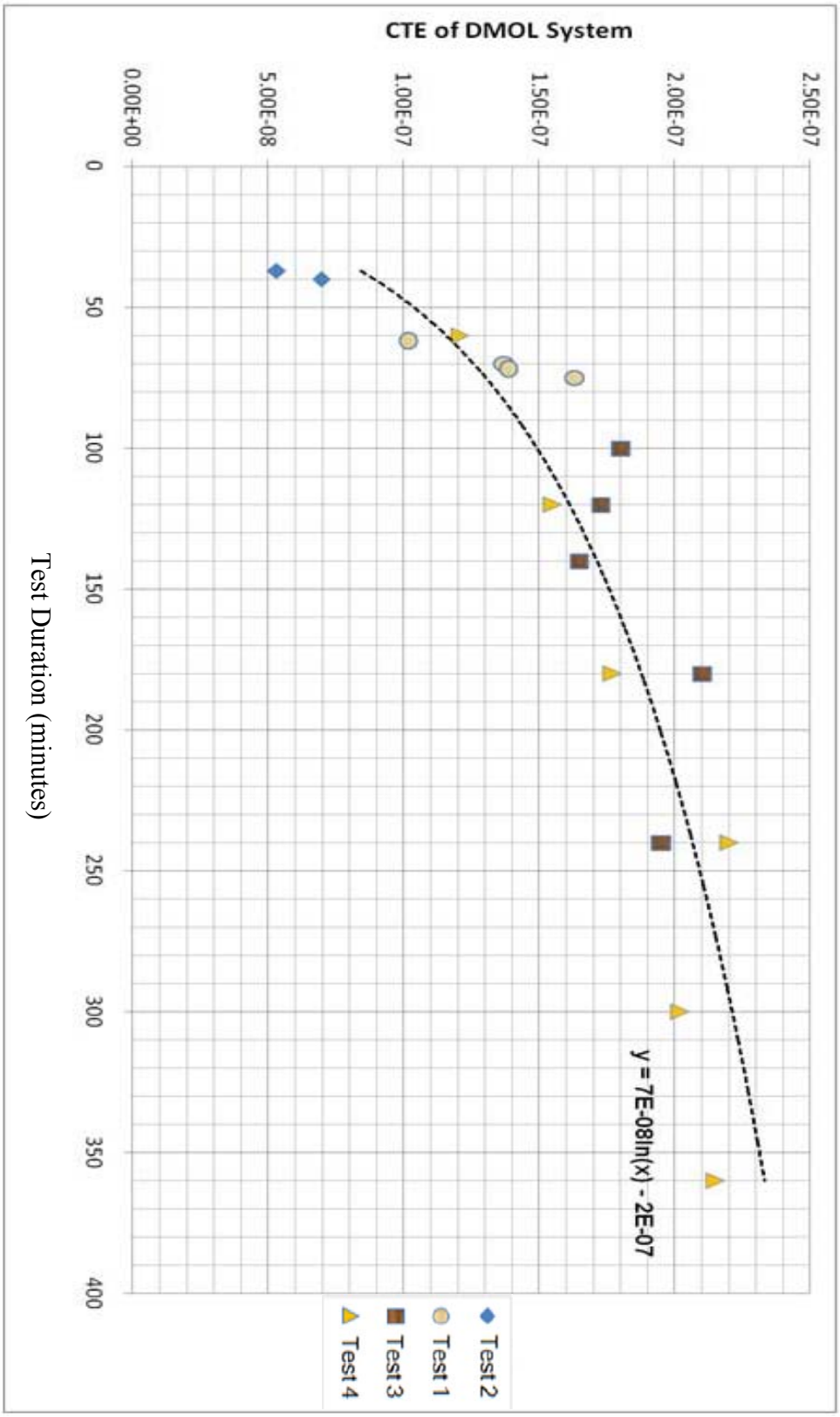

Figure 4-11. Measured overall CTE of the DMOL apparatus using Zerodur sample

Figure 4-11 indicates that overall CTE of the DMOL apparatus increases slowly as a function of test duration, which was not being considered in the previous CTE measuring results in Table 4-5. The interpolation equation to fit the curve is obtained to be: $y = (7 \times 10^{-8}) \cdot \ln x - 2 \times 10^{-7}$. Therefore, overall CTE of the DMOL apparatus from this curve can be used to correct the previous CTE tests of IM7 CFRE.

The test duration of the previous IM7 CFRE tests are provided in Table 4-7.

Table 4-7. The previous CTE of IM7 CFRE in Table 4-4 with test duration

Type	Test	Temperature Change (Celsius)	Temperature Difference (Celsius)	Test Duration (minutes)	Measured CTE (Per $^{o}C \times 10^{-6}$)
Optical Lever I	IM7 CFRE (Phase 1)	20.1-16.0	4.1	65	-0.784 ± 0.035
	IM7 CFRE (Phase 2)	16.2-20.2	4.0	75	-0.745 ± 0.036
Optical Lever II	IM7 CFRE (Phase 1)	20.2-30.2	10.0	120	-0.753 ± 0.011
	IM7 CFRE (Phase 2)	-30.3	10.1	180	-0.765 ± 0.011
	IM7 CFRE (Phase 3)	-30.1	9.9	240	-0.805 ± 0.011
	IM7 CFRE (Phase 4)	-30.1	9.9	300	-0.815 ± 0.011

Because temperature difference in Optical Lever II group (Table 4-7) and overall CTE of the DMOL setup (Table 4-6) are approximately as same: $10^{o}C$. Therefore, it is optimal to correct CTE from Optical Lever II group using the obtained overall CTE curve (Figure 4-11) or from the corresponding interpolation equation, which is $y = (7 \times 10^{-8}) \cdot \ln x - 2 \times 10^{-7}$.

Using the interpolation equation to find out the corresponding overall CTE of the DMOL apparatus (test duration at 180, 240 and 300 minutes are used):

$$y = (7\times10^{-8})\cdot\ln(180) - 2\times10^{-7} = 0.164\times10^{-6}$$

$$y = (7\times10^{-8})\cdot\ln(240) - 2\times10^{-7} = 0.184\times10^{-6}$$

$$y = (7\times10^{-8})\cdot\ln(300) - 2\times10^{-7} = 0.199\times10^{-6}$$

Therefore, these three values are the overall CTE of DMOL apparatus at three different test durations. The systematic errors are corrected if these three values are combined with measured CTE values. Table 4-8 presents the measured CTE, overall CTE of apparatus (or systematic error) and corrected CTE which are computed from first two.

Table 4-8. IM7 CFRE CTE results including both random and systematic errors

Name	Test Duration from Table 4-7 (minutes)	Measured CTE from Table 4-7 (Per $^{o}C \times10^{-6}$)	Overall CTE of Apparatus from Interpolation (Per $^{o}C \times10^{-6}$)	IM7 CFRE CTE (Per $^{o}C \times10^{-6}$)
IM7 CFRE (Phase 2)	180	-0.765 ± 0.011	0.164	-0.601 ± 0.011
IM7 CFRE (Phase 3)	240	-0.805 ± 0.011	0.184	-0.621 ± 0.011
IM7 CFRE (Phase 4)	300	-0.815 ± 0.011	0.199	-0.616 ± 0.011
			Average:	-0.613 ± 0.011

Therefore, using the average value, the final corrected CTE value including both random and systematic errors is equal to: (-0.613 ± 0.011) $\times10^{-6}$ per ^{o}C.

4.8 Discussion

In this chapter, the double-mirror optical lever (DMOL) has been introduced. The DMOL method is an improvement upon the single-mirror optical lever (SMOL) because the DMOL method provides multiple reflected points on the screen (Figure 4-3) which significantly increase the magnification of the setup and consequently provides higher resolution. Also it is a differential method having its own reference so that it reduces the measurement error resulting from small laser pointer disturbances. By observing and recording the point motions during the test, the deformation of the sample can be indirectly calculated based on the derived equations (Eq. 4-1~Eq. 4-9).

By enclosing both the test component and the reference standard in the same temperature-controlled chamber, spatial temperature gradients are avoided because the air temperature is changed sufficiently slowly and kept within a tolerance about ± 0.5 ^{o}C. Figure 4-8 demonstrates the measured air temperatures in the chamber. Although the air temperature in the chamber has a deviation about ± 0.5 ^{o}C, due to the sample's low heat conductivity and air's low heat transfer, the metering rod would be expected to respond more slowly to temperature swings compared to the values from electronic thermometers at high, medium and low vertical positions.

Despite the fact that the reference standard "fused quartz rod" used in the test has a very low CTE of between 0.40×10^{-6} per ^{o}C and 0.56×10^{-6} per ^{o}C, precise knowledge of the CTE of the reference standard is mandated because accurate determination of ultra low CTE sample such as IM7 CFRE depends upon the deformation of the reference standard. Nevertheless, this issue is resolved by finding the overall CTE of the DMOL apparatus (or systematic errors). Then this additional CTE is used to correct the measured

CTE. The overall CTE of the DMOL apparatus is calibrated using a known-CTE Zerodur rod as a test sample in the setup. Finally, the overall CTE value of the DMOL apparatus (Figure 4-11) is between 1.95×10^{-7} and 2.15×10^{-7} per ^{o}C. Three measured CTE values at 180, 240 and 300 minutes with about 10 ^{o}C temperature change (Table 4-7) are used to determine the CTE of the DMOL apparatus. Finally, the corrected CTE value of IM7 CFRE rod is found to be: $(-0.613 \pm 0.011) \times10^{-6}$ per ^{o}C which is about 20% less than the previous measured CTE value from Table 4-5. This corrected value is close to $- 0.64\times10^{-6}$ per ^{o}C from Hexcel technical data sheets.

In summary, DMOL appears to be a practical, reliable and repeatable method for measurement of environmentally-induced small deformations of large telescope components. The CTE of carbon fiber reinforced epoxy (CFRE) rod has been obtained using the DMOL method.

Chapter 5

Experiment III: Measurement of Coefficient of Moisture Expansion Using Double-Mirror Optical Lever (DMOL)

5.1 Introduction

Composite structural materials applied to space components are often made of graphite/epoxy structures using high stiffness graphite fibers (> 55×10^{-6} psi tensile modulus) and an aerospace grade low-outgassing epoxy. Normally, these epoxy resins absorb substantial quantities of water (approximately up to 3.5%) in typical room temperature environments and then this moisture desorbs in space and results in substantial shrinkage of the composite structure [39].

In practice, it is difficult to achieve near-zero Coefficient of Moisture Expansion (CME) values because of relatively slow and anisotropic mass transfer and adsorption effects [40]. Therefore, moisture adsorption/desorption laminate shrinkage remains a problem. After the development of new technological skills, this problem can be addressed by metallic alloy coating, or bonding aluminum foil to the finished structures.

However, these techniques result in increased weight, increased laminate coefficient of expansion limit the size of component which needs to be protected [39].

In the Chapter 4, a double-mirror optical lever (DMOL) was introduced for determining the coefficient of thermal expansion (CTE) of carbon fiber reinforced epoxy (CFRE) telescope components. The results from Chapter 4 indicate that the DMOL setup is feasible and repeatable for ultra low CTE measurement of CFRE. Because the DMOL setup has the two main advantages: larger magnification for observation and differential measurement to avoid disturbances, it is also suitable to employ this technique to measure the Coefficient of Moisture Expansion (CME). The sample in the CME measurement is AS4 CFRE rod. The rod was made from rolled-up pre-pregnated resin cloth, which is 32% resin, 68% carbon fiber.

This chapter describes the procedures for measuring the CME of carbon fiber reinforced epoxy (CFRE) using the same experimental setup mentioned in the Chapter 4. Results with error analysis are also provided for the CME measurement.

5.2 Operating Procedure

The DMOL setup in an environmental chamber is well-suited for CME measurement. In the CME experiments, two identical pultruded AS4 CFRE rods are first saturated in room-temperature (20.0 ^{o}C) water for several days and then placed in the constant-temperature (20.0 ± 0.5^{o}C) environmental chamber for the moisture desorption process. The first rod is placed in the DMOL dilatometer to measure the sample's strain as a function of exposure time. The second rod is also placed in the environmental

chamber and is weighed periodically using an accurate scale (Figure 5-1) to determine sample's moisture content change (desorption) as a function of exposure time.

Figure 5-1. Measuring the weight of pultruded AS4 CFRE rod
using an accurate scale (±0.01g)

Two trials are conducted for determining the CME of the pultruded AS4 CFRE. In the first trial (Test-1), the saturation time is three days (72 hours), and the measured results of strain and moisture desorption verse exposure time are shown in Figure 5-3 and Figure 5-5 respectively. As for the second trial (Test-2), the saturation time is four days (96 hours), and the measured results of strain and moisture desorption verse exposure time are shown in Figure 5-4 and Figure 5-5 respectively.

During these two trials (Test-1 and Test-2), the environment chamber is kept at constant temperature (room temperature, 20.0 ± 0.5^{o}C). However, it does not provide control of the humidity in the environmental chamber. Thus, systematic errors due to the non-uniform humidity exist in the CME test.

Therefore, it is necessary to keep a record of relative humidity (RH) which reflects the ratio of amount of water vapor in the air at a specific temperature to the maximum

amount that the air could hold at that temperature [41]. The recorded results during the CME tests are shown in Figure 5-2.

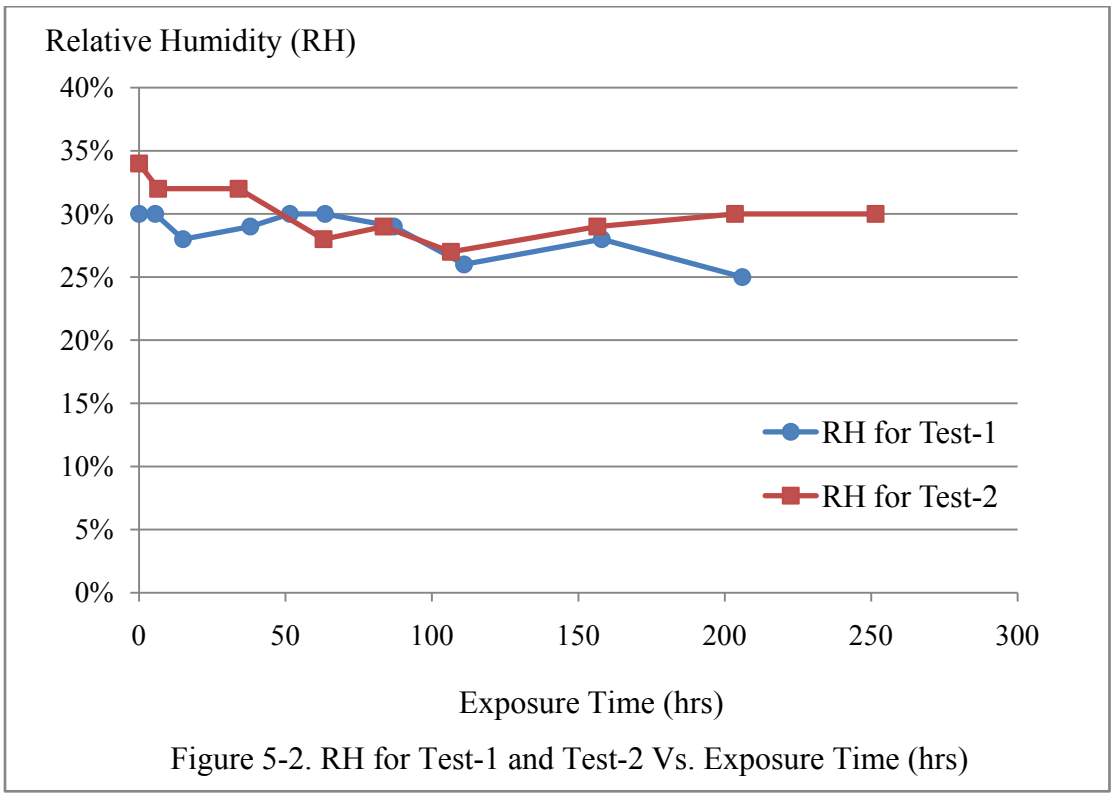

Figure 5-2. RH for Test-1 and Test-2 Vs. Exposure Time (hrs)

Figure 5-2 shows that both tests exhibit moderate changes of relative humidity (RH) between 25% and 35%. The average RH for Test-1 and Test-2 are equal to 28.5% and 30.1 % respectively. Although the RH value varies along with exposure time of CME tests, it is acceptable to use the average RH as the test condition because the RH fluctuation is relatively small (within 10%) and the sample's moisture desorption process is very slow. Therefore systematic errors due to non-uniform humidity in the CME test can be assumed to be neglectable.

In summary, the CME test conditions for Test-1 and Test-2 are:

(1) Test-1: RH=29% and temperature = 20.0 ^{o}C;

(2) Test-2: RH=30% and temperature = 20.0 ^{o}C.

Actually, because their RH values are very similar, Test-1 and Test-2 can be considered to have almost the same environmental conditions.

5.3 CME Experimental Results from DMOL

Although systematic errors appear to be negligible in the DMOL CME tests, it is still necessary to consider the random errors. The same process for evaluating uncertainty due to random errors was shown in Chapter 3, Section 3.5.1 and Chapter 4, Section 4.7.1. Similarly, uncertainty propagation is used as follows. As a calculation example, the measuring data "Test-1 Number 2" from Table 5-2 is used in Table 5-1 for calculating uncertainty propagation.

In the CME tests, Optical Lever II is used for measuring sample's strain.

Table 5-1. Measured values in "Test-1 Number 2" with their estimated uncertainties

Notation	Definition	Measured Value (cm)	Known Uncertainties (cm) (systematic errors)
ε	Sample's Strain	／	／
d	Distance between two mirror footings	0.351	± 0.00254
OE	Distance between O and E	58.6	± 0.3
O'E'	Distance between O' and E'	55.7	± 0.3
L	Distance between the beam-splitter and screen (see Figure 4-2)	461.2	± 1.0
P	Sample's original length	76.9	± 0.3

According to Eq.4-8, the sample's strain:

$$\varepsilon = \frac{d}{(2L)\times P}\cdot\frac{O'E'-OE}{5} \qquad \text{Eq. 5-1}$$

Using the same process (Chapter 3, Section 3.5.1 and Eq. 3-11) for uncertainty calculation:

$$[u\{\varepsilon\}]^2 = \left[u\left\{\frac{d}{(2L)\times P}\cdot\frac{O'E'-OE}{5}\right\}\right]^2$$

$$= \left[\frac{d}{(2L)\times P}\cdot\frac{O'E'-OE}{5}\right]^2 \times$$

$$\left[\left(\frac{u\{d\}}{d}\right)^2 + \left(\frac{\frac{1}{5}\cdot u\{O'E'-OE\}}{\frac{1}{5}\cdot(O'E'-OE)}\right)^2 + \left(\frac{u\{2L\}}{2L}\right)^2 + \left(\frac{u\{P\}}{P}\right)^2\right]$$

$$= \varepsilon^2\times\left[\left(\frac{u\{d\}}{d}\right)^2 + \left(\frac{u\{O'E'\}^2+u\{OE\}^2}{O'E'-OE}\right)^2 + \left(\frac{2u\{L\}}{2L}\right)^2 + \left(\frac{u\{P\}}{P}\right)^2\right],$$

which yields,

$$u\{\varepsilon\} = \varepsilon\times\sqrt{\left(\frac{u\{d\}}{d}\right)^2 + \left(\frac{u\{O'E'\}^2+u\{OE\}^2}{O'E'-OE}\right)^2 + \left(\frac{u\{L\}}{L}\right)^2 + \left(\frac{u\{P\}}{P}\right)^2}.$$

Taking the data "Test-1 Number 2" from Table 5-2 as an example,

$$u\{\varepsilon\} = \frac{(0.351)}{(2\times 461.2)\times 76.9}\cdot\frac{(55.7-58.6)}{5}\times$$

$$\sqrt{\left(\frac{0.00254}{0.351}\right)^2 + \left(\frac{0.3^2+0.3^2}{55.7-58.6}\right)^2 + \left(\frac{1.0}{461.2}\right)^2 + \left(\frac{0.3}{76.9}\right)^2}$$

$$= - 2.87\times10^{-6} \times \sqrt{(7.24\times10^{-3})^2 + (0.06)^2 + (2.17\times10^{-3})^2 + (3.9\times10^{-3})^2}$$

$$= - 0.18\times10^{-6}.$$

Based on t he calculation of the propagation of uncertainty above and the measured data, Table 5-2 and Table 5-3 show the measured strain of the pultruded AS4 CFRE and also random errors in Test-1 and Test-2. Accordingly, Figure 5-3 and Figure 5-4 demonstrate the strain change as a function of exposure time for Test-1 and Test-2.

Weight loss of the pultruded AS4 CFRE in Test-1 and Test-2 are recorded in Table 5-4, which can be also considered as the moisture desorption because the only decrease in the samples is the water content.

Comparing Figure 5-3 and Figure 5-4, it is apparent that Test-2 has a relatively larger strain change than Test-1 during the whole test. The reason is that the initial saturation time of sample in Test-2 was longer than that of Test-1. Therefore, under almost the same environmental conditions, the sample in Test-2 loses more moisture and thus shrinks more than the sample in Test-1. Also this explains why in Figure 5-5 the moisture desorption in Test-2 is more than in Test-1.

Table 5-2. Strain and according error $u\{\varepsilon\}$ for pultruded AS4 CFRE, Test-1

Number	Time (hrs)	d (cm)	OE (cm)	O'E' (cm)	L (cm)	P (cm)	Strain ε Per $^{o}C \times 10^{-6}$	$u\{\varepsilon\}$ Per $^{o}C \times 10^{-6}$
1	0	0.351	58.6	58.6	461.2	76.9	0	0
2	5.5	0.351	58.6	55.7	461.2	76.9	- 2.87	± 0.18
3	15	0.351	58.6	54.3	461.2	76.9	- 4.26	± 0.19
4	38	0.351	58.6	53.0	461.2	76.9	- 5.54	± 0.20
5	51.5	0.351	58.6	52.7	461.2	76.9	- 5.84	± 0.20
6	63.5	0.351	58.6	52.2	461.2	76.9	- 6.33	± 0.20
7	87	0.351	58.6	51.9	461.2	76.9	- 6.63	± 0.20
8	111	0.351	58.6	51.4	461.2	76.9	- 7.13	± 0.21
9	158	0.351	58.6	50.8	461.2	76.9	- 7.72	± 0.21
10	206	0.351	58.6	50.5	461.2	76.9	- 8.02	± 0.21

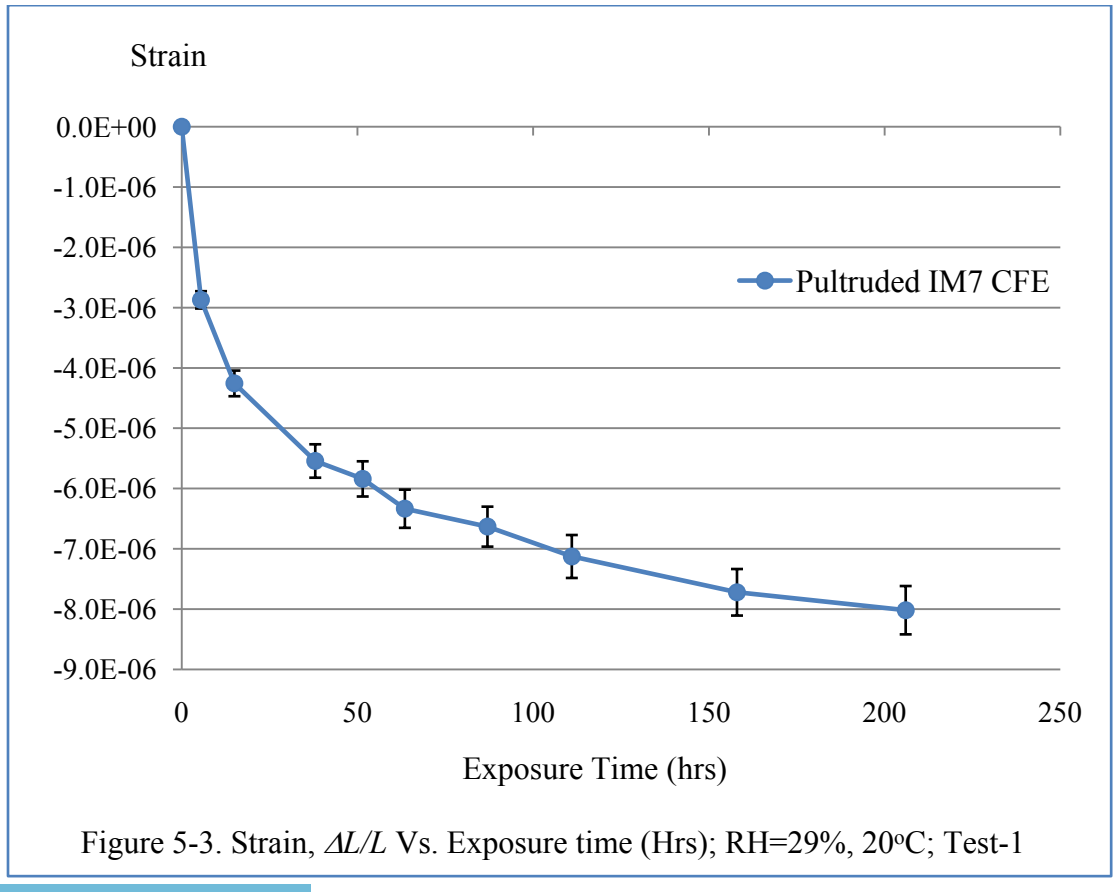

Figure 5-3. Strain, $\Delta L/L$ Vs. Exposure time (Hrs); RH=29%, 20°C; Test-1

Table 5-3. Strain and according error $u\{\varepsilon\}$ for pultruded AS4 CFRE, Test-2

Number	Time (hrs)	d (cm)	OE (cm)	O'E' (cm)	L (cm)	P (cm)	Strain ε Per $^{o}C \times 10^{-6}$	$u\{\varepsilon\}$ Per $^{o}C \times 10^{-6}$
1	0	0.351	65.5	65.5	461.2	76.9	0	0
2	6.5	0.351	65.5	61.6	461.2	76.9	- 3.86	± 0.19
3	34	0.351	65.5	59.3	461.2	76.9	- 6.14	± 0.20
4	63	0.351	65.5	56.2	461.2	76.9	- 9.20	± 0.22
5	83.5	0.351	65.5	55.4	461.2	76.9	- 9.99	± 0.23
6	106.5	0.351	65.5	54.6	461.2	76.9	- 1.08	± 0.24
7	156.5	0.351	65.5	53.1	461.2	76.9	- 12.27	± 0.26
8	203.5	0.351	65.5	51.6	461.2	76.9	- 13.76	± 0.27
9	251.5	0.351	65.5	50.8	461.2	76.9	- 14.55	± 0.28

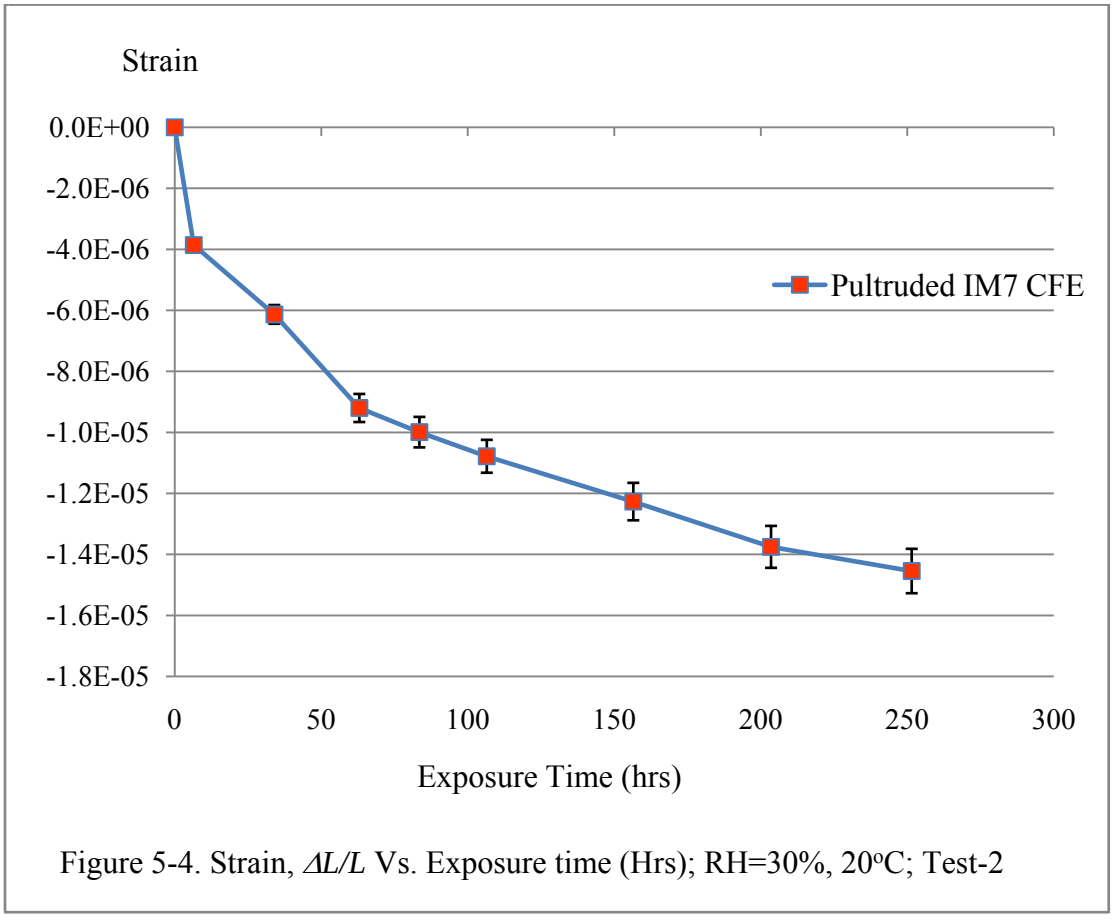

Figure 5-4. Strain, $\Delta L/L$ Vs. Exposure time (Hrs); RH=30%, 20°C; Test-2

Table 5-4. Weight loss and according moisture desorption in Test-1 and Test-2

Test-1 Number	Time (hrs)	Weight (gram)	Moisture Desorption %	Test-2 Number	Time (hrs)	Weight (gram)	Moisture Desorption %
1	0	60.01	0.000	1	0	60.47	0.000
2	5.5	59.99	-0.033	2	6.5	60.44	-0.050
3	15	59.98	-0.050	3	34	60.42	-0.083
4	38	59.97	-0.067	4	63	60.4	-0.116
5	51.5	59.96	-0.083	5	83.5	60.39	-0.132
6	63.5	59.95	-0.100	6	106.5	60.37	-0.165
7	87	59.95	-0.100	7	156.5	60.36	-0.182
8	111	59.94	-0.117	8	203.5	60.34	-0.215
9	158	59.93	-0.133	9	251.5	60.33	-0.232
10	206	59.93	-0.133				

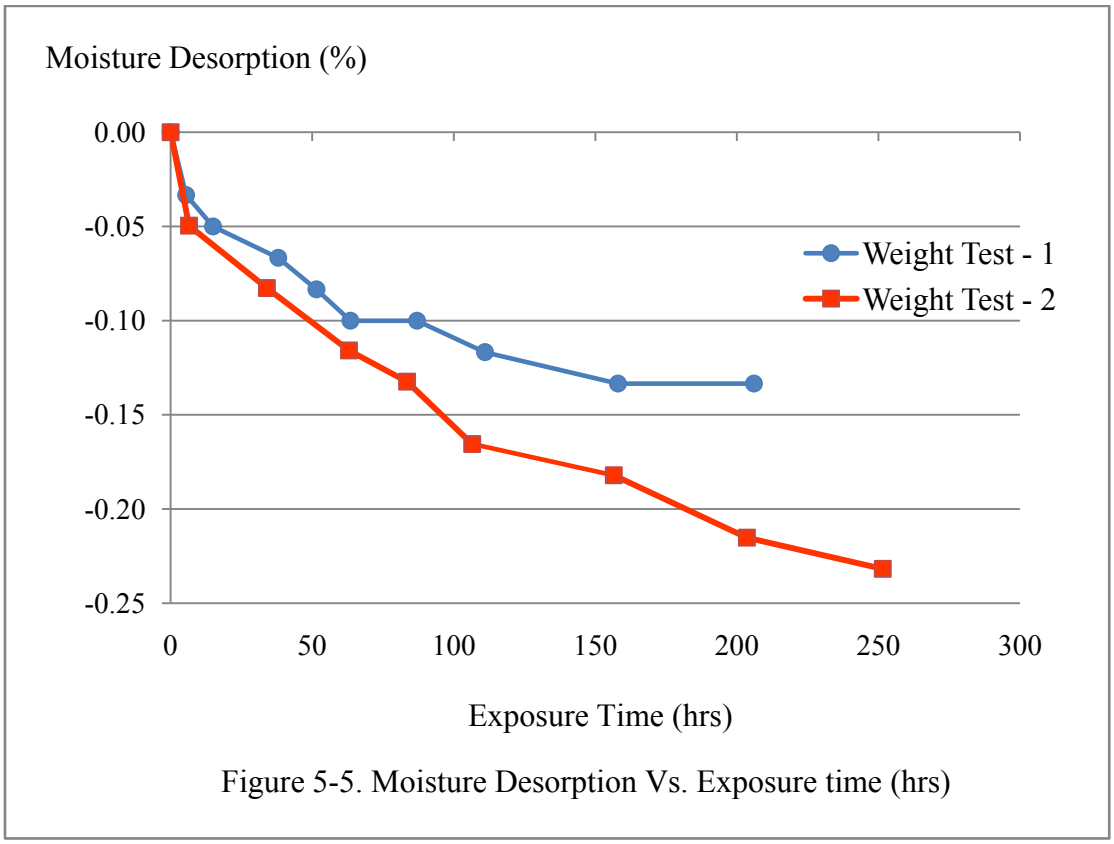

Figure 5-5. Moisture Desorption Vs. Exposure time (hrs)

The CME of the sample is determined by determining the slope of line fitted to the data points in Figure 5-6 [40]. The CME of pultruded AS4 CFRE is found to be 61.6×10^{-6} m/m per fraction moisture content under the condition of relative humidity= 29%~30% and temperature = 20°C.

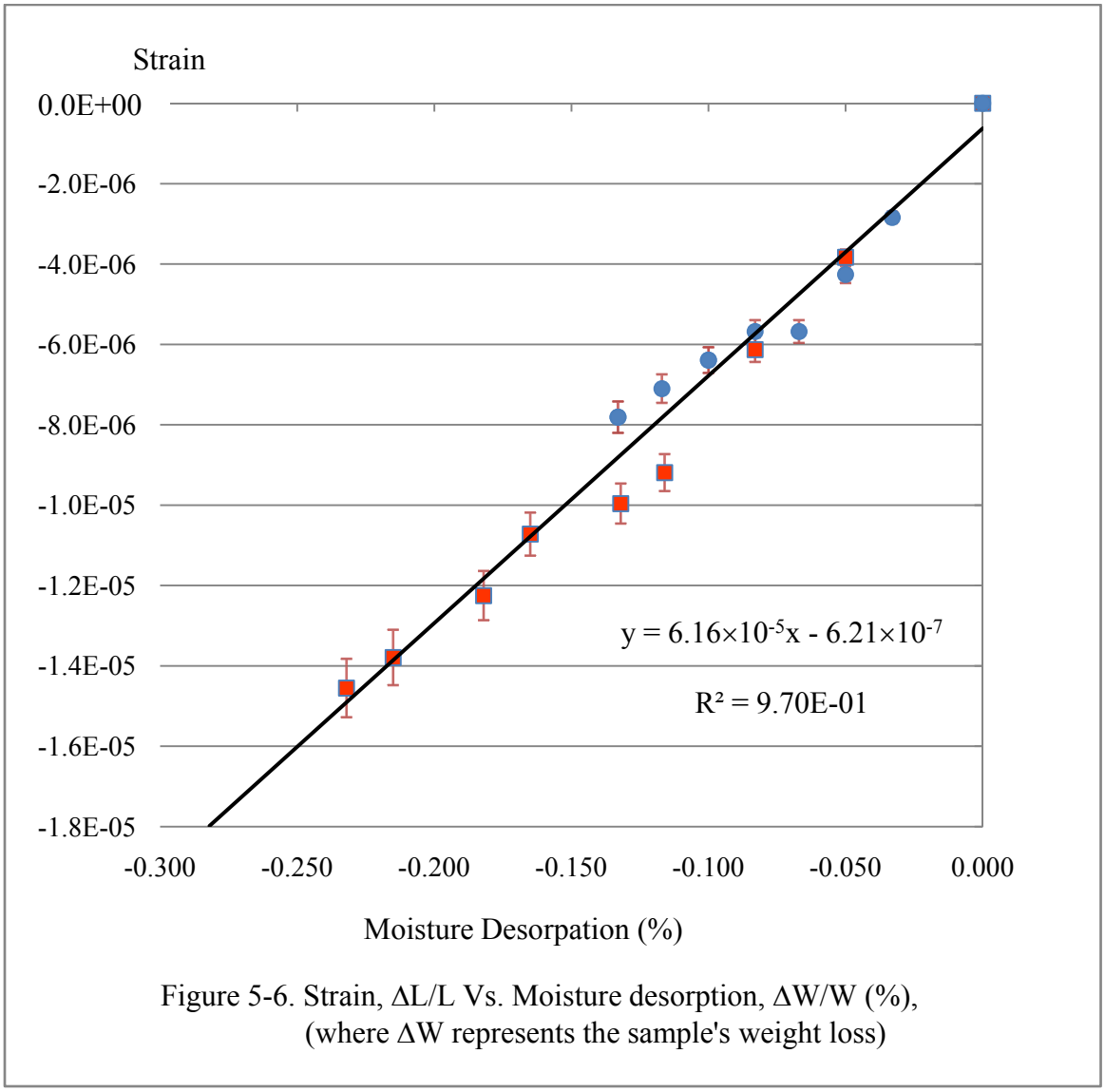

Figure 5-6. Strain, ΔL/L Vs. Moisture desorption, ΔW/W (%), (where ΔW represents the sample's weight loss)

5.4 Discussion

The CME tests in this chapter indicate that this DMOL dilatometer is suitable for measurement of coefficient of moisture expansion (CME) of carbon fiber reinforced epoxy (CFRE) telescope components. Two independent tests (Test-1 and Test-2) were conducted to determine the CME of pultruded AS4 CFRE under almost the same environmental conditions: one is RH = 29%, temperature = 20^{o}C; another one is RH = 30%, temperature = 20^{o}C. Comparison of Test-1 in Figure 5-3 and Test-2 in Figure 5-4 shows that the strain-change ratio of the latter is faster than the former. The reason for this is that the saturation time of Test-2 was four days (96 hours) which is 24 hours longer than Test-1. As a result, Test-2 lost the moisture content faster than Test-1 under the almost same RH and temperature conditions. The same explanation can be used for the different moisture desorption ratios in Figure 5-5.

Finally, the CME value of the pultruded AS4 CFRE is found to be 61.6×10^{-6} m/m per fraction moisture content by weight using these two groups of data in Figure 5-6. In fact, this value indicates that moisture desorption due to the laminate shrinkage process in a real environmental situation should be considered as an important factor in large composite components.

Chapter 6

Conclusions

6.1 Summary and Conclusions

Due to the need for applying high-performance composite materials to large-sized structural components in the spacecraft and telescopes, the development of more dimensionally stable composite structures is crucial. The essential precondition for developing high-quality stable composite structures is to explore the properties of composite components, especially the thermal and moisture induced deformations due to the environmental changes.

This thesis introduced two methods of measurement of environmentally-induced deformations of telescope components. The first method is the single-mirror optical lever (SMOL), which was employed to measure the coefficient of thermal expansion (CTE). The second is the double-mirror optical lever (DMOL), which was used to measure both the CTE and the coefficient of moisture expansion (CME).

In the SMOL tests, the deformation of the sample was amplified using an optical lever theory and then computed by observing the motion of a laser point on the screen. The temperature of the sample was controlled by circulating water, from room

temperature (approx. 20 ^{o}C) to ice temperature (approx. 0 ^{o}C). Although the random errors in the SMOL measurement were in the range of ± 15%, the systematic errors for the SMOL apparatus were too large to neglect (> 100% of the measurement). ANSYS modeling in Section 3.6 indicates the concrete floor has a significant effect upon the measurement. Therefore, the SMOL method did not provide a sufficiently reliable way to measure the CTE of materials such as aluminum, steel, and IM7 carbon fiber reinforced epoxy (CFRE). Also, it turns out that the SMOL method is certainly not sufficiently feasible to measure the CME, which requires long duration tests.

The double-mirror optical lever (DMOL) method was developed to correct the flaws with the SMOL method. The DMOL is basically a two-mirror arrangement for generating multiple reflected laser points on the screen. Because it has a series of points for observation, the magnification is increased to 5 or 6 times as much as the SMOL method. Also, because differential point motions on the screen are caused by sample's deformation, environmental disturbances such as small changes in laser pointer location do not cause significant errors in measurement. Finally, the use of a temperature-controlled environmental chamber ensured a uniform spatial temperature of the sample, which importantly eliminated systematic errors from the heat transfer between the sample and the surroundings. In the end, the final corrected CTE value of IM7 CFRE rod including both random and systematic errors, is found to be: $(-0.613 \pm 0.011) \times 10^{-6}$ per ^{o}C.

The CME measurement was also conducted using the DMOL method with its high magnification and low random and systematic errors. The value of the CME was determined by using figures of strain versus duration and moisture desorption versus duration. The long test duration (200 hours for Test-1 and 250 hours for Test-2) ensured

that the sample's deformation was large enough for observation and calculation. Finally, the CME value of pultruded AS4 CFRE is found to be 61.6×10^{-6} m/m per fraction moisture content by weight.

6.2 Future Work

The research for CTE and CME of the CFRE materials is ongoing as the Air Force Research Laboratory continues to have an interest in this research.

Suggestions for future research include:

(1) Although the new DMOL method is reliable and repeatable for measuring CTE and CME of CFRE, switching the optical lever I/II may cause a corresponding change of the footing distance *d*. This problem indicates that the DMOL apparatus' CTE (or DMOL's systematic errors) we calibrated using a known-CTE Zerodur in Chapter 4, Section 4.7.2 is not as same as the DMOL apparatus' CTE we used for the previous CTE tests.

(2) Due to the limited resources, the fabrication of the DMOL apparatus was not very high quality. Also the Optical Lever I and II need to be improved. More careful fabrication work is necessary on, for instance, the footings and beam-splitter to ensure the stability during long duration tests.

(3) Systematic errors due to the non-uniform humidity in the CME tests are assumed to be negligible. However, it does have effect to some degree. Therefore, having a humidity-controlled environmental chamber or devices will be very helpful for the CME tests.

(4) Further investigation into thermally tunable components is needed to determine the materials and fabrication methods of the final structural design. It is advantageous to be

able to “tune” a structure for a particular desired CTE than to have a non -tunable structure with near-zero CTE.

(5) It would be useful to adapt these techniques for application to a real telescope in its working environment.

References

[1] Gerstle, W. H., Roybal, F. A., McGraw, J. T. and Williams, W. T. "Structural Design of a Unique Passive Telescope." *Measurement Science and Technology*, ASCE, 40830(188), Pages 148-156, 2006

[2] Roybal, F. A. "Structural Design of A Passive Transit Telescope." *Master of Science in Civil Engineering*, University of New Mexico, 2007

[3] Kern Swiss Instruments - Swisstek Inc. *http://www.swisstek.com/kern_swiss.htm*

[4] James, J. D. , Spittle, J. A., Brown, S. G. R. and Evans, R. W. "A Review of Measurement Techniques for the Thermal Expansion Coefficient of Metals and Alloys at Elevated Temperatures." *Institute of Physics Publishing*, Vol.12, Number 3, Pages R1-R15, 2001

[5] American Society for Testing and Materials ASTM E 228, 1999

[6] Joseph, V. "A Vitreous Silica Tube Dilatometer for the Measurement of Thermal Expansion of Solids from -195 to 1000° C." *Journal of Materials Science*, Vol.14, Number 2, Pages 371-378, 2004

[7] Joseph, V. "Polycrystalline Alumina for Tube Dilatometer." *ISA Trans*. Vol.16, Number 81, 1977

[8] Valovič, Š., Štubňa. "Calibration of the Horizontal Pushrod Dilatometer." *Thermophysics*. Pages 126-131. 2002

[9] ASM Ready Reference: "Thermal Properties of Metals." 2002

[10] ISO 7991: "Glass - Determination of Coefficient of Mean Linear Thermal Expansion," 1987

[11] Upadhyaya, A., Griffo, A. and German, R. M. "Thermal Conductivity 24—Thermal Expansion." Lancaster, PA: Technomic, Pages 393-404, 1999

[12] American Society for Testing and Materials ASTM E 289-99, 1999

[13] Bishnu, P. "Fundamentals of Fibre Optics in Telecommunication and Sensor Systems." *Delhi: New Age International Ltd*, Page 663 (read section 3). ISBN 8122404693. 1992, 2005

[14] Hernandez, G. "Fabry-Perot Interferometers." *SCIENCE*,Vol.243, Number 4896, Page 1376, 1989

[15] Wikipedia. "Fabry-Perot Interferometers." *http://en.wikipedia.org/wiki/Fabry%E2%80%93P%C3%A9rot_interferometer*

[16] Wikipedia. "Fizeau Interferometer." *http://en.wikipedia.org/wiki/Fizeau_interferometer*

[17] Preston, S. D. "Thermal Expansion of Measurement on Boron Carbide and Europium Sesquioxide by Laser Interferometry." *High Temperature – High Pressure*, Vol.12, Pages 411-446, 1980

[18] "Linear Thermal Expansion of Rigid Solid with Interferometry." ASTM Standards E289-94b, 1994

[19] Jinhu, H. and Tianxiang, M. "The Application of Moire Interferometry in the Measurement of Displacement Field and Strain Field at Notch-tip and Crack-tip." *Acta Mechanica Sinica*, Vol.7, Number 4, 1991

[20] Se, Y. Y., and Soon-Bok, L. "Realization of High Sensitivity Displacement Field from Moiré Interferometer with Rough Phase Shifting Mechanism and Pattern Matching Technique." *Optics and Lasers in Engineering*, Vol.43, Issue 6, Pages 721-736, 2005

[21] Wikipedia, "Michelson interferometer." *http://hyperphysics.phy-astr.gsu.edu/hbase/phyopt/michel.html*

[22] Wikipedia, "Strain gauge." *http://en.wikipedia.org/wiki/Strain_gauge*

[23] Touloukian, Y. S., Kirby, R. K. and Taylor, R. E. "Thermophysical Properties of Matter." *Thermal Expansion, Metallic Elements and Alloys.* Vol.12 Page 14a, 1975

[24] Vishay Micro-Measurements System 7000 *http://www.vishay.com/company/press/releases/2008/080416system7000/*

[25] Wolff, E. G. "Introduction to the Dimensional Stability of Composite Materials." DEStech Publications, Inc., Lancaster, Pennsylvania. 2004

[26] Barron, T. H. "Cindas Data Series on Material Properties." *Thermal Expansion of Solids*, Materials Park, OH: ASM International, Vol. I-4, Chapter 1. Page 5. 1998

[27] Krumweide, G. C., Chamberlin, D. N., and Derby, E. A. "Measuring Thermal Expansion in Large Composite Structures." Composite Optics, *International SAMPE Technical Conference*, 1986

[28] ANSYS, Inc. *http://www.ansys.com/*

[29] Wikipedia, "Small-angle approximation" *http://en.wikipedia.org/wiki/Small-angle_approximation*

[30] Touloukian, Y. S., Kirby, R. K., Taylor, R. E. and Desai, P. D. "Thermophysical Properties of Matter, Thermal Expansion, Metallic Elements and Alloys" New York: IFI-Plenum, Vol.12. Page 4a. 1975

[31] Hexcel IM7 (5000) Carbon Fiber Product Data Sheet, March 2002 *http://www.hexcel.com/NR/rdonlyres/BD219725-D46D-4884-A3B3-AFC86020EFDA/0/HexTow_IM7_5000.pdf*

[32] Error Analysis. *http://www.physics.uc.edu/~bortner/labs/Physics%20Lab%20web%20site/Appendix%201/Appendix%201%20Error%20Analysis%20htm.htm*

[33] Wikipedia, "Random Errors," *http://en.wikipedia.org/wiki/Random_error*

[34] Wikipedia, "Systematic Error," *http://en.wikipedia.org/wiki/Systematic_error*

[35] Hugh W. Coleman, W. Glenn Steele, "Experimentation and uncertainty analysis for engineers," *Wiley-Interscience*; 2 edition (January 25, 1999)

[36] NIST, Manufacturing Engineering Laboratory, Engineering Metrology Toolbox *http://emtoolbox.nist.gov/Temperature/Slide14.asp*

[37] Wikipedia, "Fused Quartz," *http://en.wikipedia.org/wiki/Fused_quartz*

[38] Valley Design Corp. GE 124 Fused Quartz 100 mm Wafers to SEMI Specifications, *http://www.valleydesign.com/ge124-av.htm*

[39] Blair, C. and Zakrzewski, J. "Coefficient of Thermal and Moisture Expansion and Moisture Absorption for Dimensionally Stable Quasi-Isotropic High Modulus Graphite Fiber/Epoxy Composites." *Advances in Optical Structure System*, Vol.1303, Pages 524-535, 1990

[40] Wolff, E. G. "Moisture and Viscoelastic Effects on the Dimensional Stability of Composites." *Proceeding of SPIE*, Vol.1335, Pages 70-79, 1990

[41] Wikipedia, "Relative Humidity," *http://en.wikipedia.org/wiki/Relative_humidity*